Timing Jitter in Ultra-Wideband (UWB) Systems

A Thesis
Presented to
The Academic Faculty

by

Uzoma Onunkwo

In Partial Fulfillment
of the Requirements for the Degree
Doctor of Philosophy

School of Electrical and Computer Engineering
Georgia Institute of Technology
May 2006

Timing Jitter in Ultra-Wideband (UWB) Systems

Approved by:

Professor Ye (Geoffrey) Li, Advisor
School of Electrical and Computer Engineering
Georgia Institute of Technology

Professor Mary Ann Ingram
School of Electrical and Computer Engineering
Georgia Institute of Technology

Professor Gregory D. Durgin
School of Electrical and Computer Engineering
Georgia Institute of Technology

Professor Mark A. Richards
School of Electrical and Computer Engineering
Georgia Institute of Technology

Professor Xingxing Yu
School of Mathematics
Georgia Institute of Technology

Date Approved: March 15, 2006

To my loving parents and my sweetheart, Ifeoma,

for their invaluable encouragement and prayers

ACKNOWLEDGEMENTS

I will like to express my utmost gratitude to my advisor, Prof. Ye (Geoffrey) Li. He has been a tremendous advisor in every sense of the word, especially in regards to my studies and research work. He has guided me through the hard-fought years of developing the essential skills of independent research. I am ever grateful for his invaluable advice and encouragement, and all the special time and diligence he has put in guiding me in my research and publications.

I will like to thank my thesis committee members, Prof. Mary Ann Ingram, Prof. Gregory D. Durgin, Prof. Mark A. Richards, and Prof. Xingxing Yu. Their remarks and comments during and after my proposal defense have been very valuable in improving the quality of my thesis.

I am also very grateful to the past and present members of the Information Transmission and Processing (ITP) Laboratory: Hua Zhang, Jianxuan Du, Jingnong Yang, Taewon Hwang, Guocong Song, Jian Zhu, and Ghurumuruhan Ganesan. They have been helpful in my research by their numerous technical discussions including important issues concerning my work. They have also been a great bunch of friends to hang out with over the years.

Lastly, but not the least, I will like to thank my loving dad and mom, and also my lovely fiancée, Ifeoma, for who they are to me. This thesis is dedicated to them.

TABLE OF CONTENTS

LIST OF TABLES

LIST OF FIGURES

SUMMARY

Ultra-wideband wireless communication has recently attracted interests due to the high data rate and covertness it provides. This results from the large bandwidth and low spectral mask ascribed for ultra-wideband communication. However, the larger bandwidth available for a UWB system inadvertently results in some atypical adversity issues not substantial in narrowband communication - more interference and higher timing jitter effect - that should be considered by communication engineers.

In traditional UWB systems (impulse radio), the need for great timing accuracy is further pronounced by the sub-nanosecond pulse widths of the transmitted signals. However, dealing with real systems means that sampling clocks at the receiver will be non-ideal. This in effect gives room for sampling offsets referred to as timing jitter. Although receiver synchronization and the mobility of receiver-transmitter relative positions can cause timing jitters too, our primary focus in this work is on clock sampling timing jitters. Timing jitters produce a noisy sequence at the receiver, which can be substantially large and result in a bad communication system unless measures are taken to mitigate this effect. Our work studies this effect in detail and provides simple and effective ways of dealing with this issue.

The incorporation of *orthogonal frequency division multiplexing* (OFDM) makes ultra-wideband systems (UWB) more immune to delay spread. However, the relatively large bandwidth compared to their narrowband counterpart results in a more pronounced timing jitter effect, namely, inter-channel interference (ICI) for OFDM-based UWB. This ICI has been shown to be directly affected by the bandwidth and RMS of the timing jitter. We have focused on this induced ICI and the worst-case effect. We have proposed and validated a number of techniques for reducing this

ICI, thereby giving system improvement in signal detection and channel estimation. These ICI reduction schemes are oversampling at the receiver and adaptive modulation techniques. Our results show that oversampling and adaptive modulation can reduce the ICI power.

Our work is extended to consider practical issues that need to address the effect of timing jitter on UWB systems. The challenge of channel estimation and signal detection due to the added dimension of multipath fading inadvertent in UWB systems makes timing jitter reduction an invaluable task.

CHAPTER 1

INTRODUCTION

Since its approval by the *Federal Communications Commission* (FCC) in 2002 [5], UWB signaling has grown rapidly in research areas on wireless communications. UWB systems are divided into two main categories – single-carrier modulation, also called impulse radio, that usually uses *pulse-position modulation* (PPM) and *pulse-amplitude modulation* (PAM), and multi-carrier modulation or *orthogonal frequency division multiplexing* (OFDM) [5, 21]. OFDM can easily deal with the delay spread caused by UWB channels. Therefore, within the IEEE 802.15.3a standardization group, OFDM, combined with time-frequency interleaving [4], has emerged as a promising candidate.

A UWB system potentially provides a high data rate over a huge bandwidth. Since the UWB pulse duration is very short, the UWB signal becomes very sensitive to sampling timing jitter, which can significantly degrade the performance of the communication system. This effect has been partly studied in [11, 13, 15, 17, 28, 42] for single-carrier based UWB systems. The effective power-spectral density of the sampled signal, under time jittered sampling, has been studied in [3,25] for the general case and in [7] for radar applications.

Timing jitter also affects the performance of OFDM communication systems, which has been analyzed in [29, 38, 44]. In [29], the authors have studied the effect of timing jitter with a low pass power spectral density. In [44], the authors have analyzed performance degradation resulting from timing jitter when OFDM is used in an *asymmetric digital subscriber line* (ADSL). However, there is no analysis of the impact of timing jitter on OFDM-based UWB systems taking into account the

relatively large bandwidth.

To reduce errors in signal detection for UWB systems, it is essential to study the effect of timing jitter at the receiver under the UWB channel characteristics. For single-carrier UWB systems, timing jitter results in distortion of the signal spectral density by affecting the correlation between the basis signals at the receiver. For OFDM-based UWB systems, timing jitter introduces ICI in the symbols. The ICI becomes larger because of the higher bandwidths for UWB systems, and hence its reduction is essential. In this work, we propose the use of oversampling and adaptive symbol modulation to reduce the ICI power.

Adaptive symbol modulation can reduce the average ICI power by exploiting the non-uniformness property of ICI over subcarriers for a correlated timing jitter process. Finally, we incorporate both ICI reduction techniques and derive the optimum performance under the Gaussian correlation and exponential correlation properties of timing jitter.

The rest of this work is organized as follows. Section 1.2 reviews the characteristics and modulation techniques of UWB systems. We then discuss the properties that make the modulation schemes amenable to signal detection in UWB communication. Chapter 2 and Chapter 3 describe the effect of timing jitter on single-carrier and OFDM-based UWB, including the theoretical bounds on timing jitter-induced ICI. Afterwards, the use of oversampling and adaptive modulation for the reduction of average ICI over noiseless channel is explored in Chapter 4. Chapter 5 then highlights the practical issues that have to cater for timing jitter in UWB, essentially channel estimation and signal detection.

1.1 UWB Systems

UWB communication is believed to have started in 1895 from the work of Guglielmo Marconi, known as the *Father of Radio* in his spark-gap transmitter. At that time,

UWB was not really a research area. It is only until recently that interests grew in this area when researchers studied the impulse response of microwave circuits [16]. UWB was first called *impulse radio*. However, today, impulse radio only refers to one type of modulation scheme in UWB communications, which will be discussed later. The underlying idea behind UWB communication is that it has relatively large bandwidth.

1.1.1 Description

UWB system, as formally defined by FCC, is referred to as radio systems whose fractional bandwidth is at least 25% of its center frequency or whose bandwidth is at least 1.5 GHz (with a minimum sub-band of 512 MHz for OFDM-based UWB) [2]. The frequency band most used for UWB systems is in the range of 3.1 to 10.6 GHz [12, 35]. Following the standards of FCC, there is a further power restriction as depicted in Fig. 1.

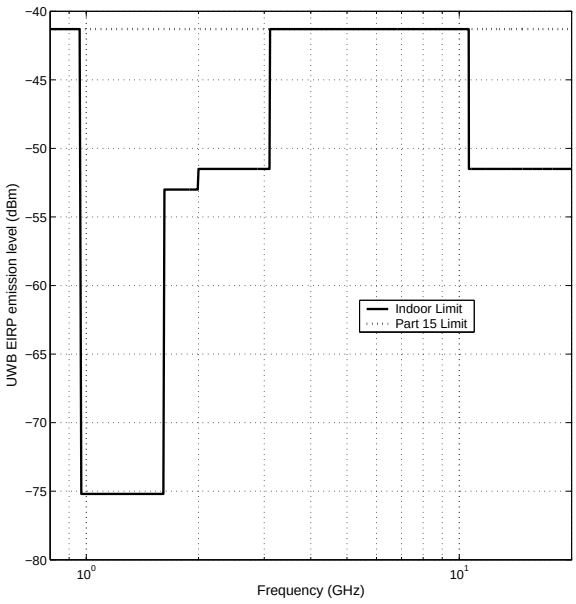

Figure 1. FCC spectral mask as it applies to UWB systems.

UWB communication is different from narrowband communication in that narrowband communications have relatively narrow bandwidth compared to its center

frequency. The *Global System for Mobile Communication* (GSM) standard is an example of a narrowband communication system. In GSM, the reverse link and forward link bands are 890-915 MHz and 935-960 MHz, respectively, which means a system with carrier frequency of about 900 MHz and bandwidth of 25 MHz (approximately 3% in fractional bandwidth). In narrowband systems, there is a need for an upconverter to convert the baseband signals to a higher frequency range for transmission, which is not necessary in UWB (impulse radio) communications.

Moreover, most narrowband systems today have bandwidth restriction to avoid interference with other users or communication systems. Therefore, licensing requirements are imposed by appropriate communications regulating authorities (e.g. FCC in the USA). On the other hand, UWB communication uses unlicensed bands. This, however, means that a restriction has to be imposed on the power level to avoid drastic impediment, in the form of interference, to existing narrowband communication systems [37].

1.1.2 Motivation

The huge and unlicensed bandwidth have been major proponents for the research works in this field. From Shannon's capacity formula, it is obvious that larger bandwidth means greater ergodic capacity. Therefore, it is an ideal tool for high data rate and short range communications, which is very desirable for multimedia applications in indoor wireless communications. Another UWB application is in location estimation. The work by Sakamoto and Sato in [36] has shown that UWB can also be used in locating targets with great precision.

As with new innovative technologies, some limitations have been detected and system designs will have to deal with these issues. One of such limitation is the effect of timing jitter inherent in the UWB definition. This is substantial as UWB employs large bandwidth thereby requiring great timing accuracy. Unlike previous cases in

narrowband communication, common clock sampling timing jitter inaccuracy with jitter root-mean-square between 15 ps and 150 ps now pose a significant problem in the error-rate performance of UWB. This problem along with its quantified effect and mitigation are what constitute the bulk of this dissertation work.

The nanosecond-short pulse widths and low power used in impulse radio make UWB signals appear as *noise* to other communication systems/users and is hence subtle to intrusion. This finds use in high security communications and highly covert communications. Therefore, UWB has been widely studied in the military field.

1.2 UWB Modulation Techniques

In order to properly examine the effect of timing jitter on UWB systems, we first describe the modulation techniques normally used with UWB. The modulation applied varies depending on the type of UWB system in consideration - impulse radio (single-carrier) or multi-carrier. Since there is an abundance of bandwidth in UWB systems, most modulation schemes applied are not geared towards spectral efficiency rather power efficiency is the primary focus.

1.2.1 Single-carrier based

There are a number of modulation schemes that can be applied to an impulse radio system. One of such scheme is *pulse-position modulation* (PPM).

1.2.1.1 Pulse-position modulation (PPM)

PPM is the scheme employed in impulse radio, a primitive UWB modulation scheme. It uses combination of short pulses to represent a symbol. We first present the basic concept of *time-hopping* (TH) PPM and then address modulation index optimization to improve the performance of TH-PPM systems.

For binary TH-PPM, the signal for the m-th user, $s^{(m)}(t)$, is represented by:

$$s^{(m)}(t) = \sum_n w^{(m)} \left(t - nT_s - b_n^{(m)} \delta \right), \tag{1}$$

where T_s is the symbol period, $b_n^{(m)} \in \{0, 1\}$ is the n-th transmitted binary data from the m-th user, δ is the modulation index, and $w^{(m)}(t)$, a spreading of basic pulses, is defined as[1]

$$w^{(m)}(t) \;\; = \;\; \sum_{l=0}^{N-1} p(t - lT_c - c_l^{(m)} \Delta_o), \tag{2}$$

$c_l^{(m)} \in \{0, 1\}$ is a spreading code unique for every user to enable efficient multiple accessing (similar to CDMA but much shorter), and Δ_o is the time shifting term associated with $c_l^{(m)}$, N is the number of pulses, $p(t)$, in a symbol duration. Each pulse (called *chip* in CDMA literature) occupies a time interval, T_c; consequently, $T_s = N \cdot T_c$. The modulation index, δ, is an important parameter for TH-PPM that can improve BER performance [32].

The pulse-shaping function most adopted for PPM is the Gaussian monocycle or its higher-order derivative although other functions can be also used. The first-order Gaussian monocycle can be expressed as

$$p(t) = \frac{A}{\sigma} \left(c - \frac{t}{\sigma} \right) e^{-0.5\left(\frac{t}{\sigma} - c\right)^2},$$

where the constant A is an amplitude normalization constant, σ is related to the width of the pulse, and c is a time-shifting term. Its time- and frequency- domain representations are shown in Fig. 2 where $c = 0$ and $2\pi\sigma = 1$ nsec. From the figure, the Gaussian pulse spreads its power over a wide range of frequency and has virtually no DC and low frequency components, which makes it suitable for UWB communication [8]. Another reason Gaussian monocycles are used extensively in literature for impulse radio communication is that they attain low bandwidth-time product of a half.

[1] If there is only one user, the superscript m will be omitted and the code sequence $\{c_l^{(m)}\}_{l=0}^{N-1}$ will be ignored.

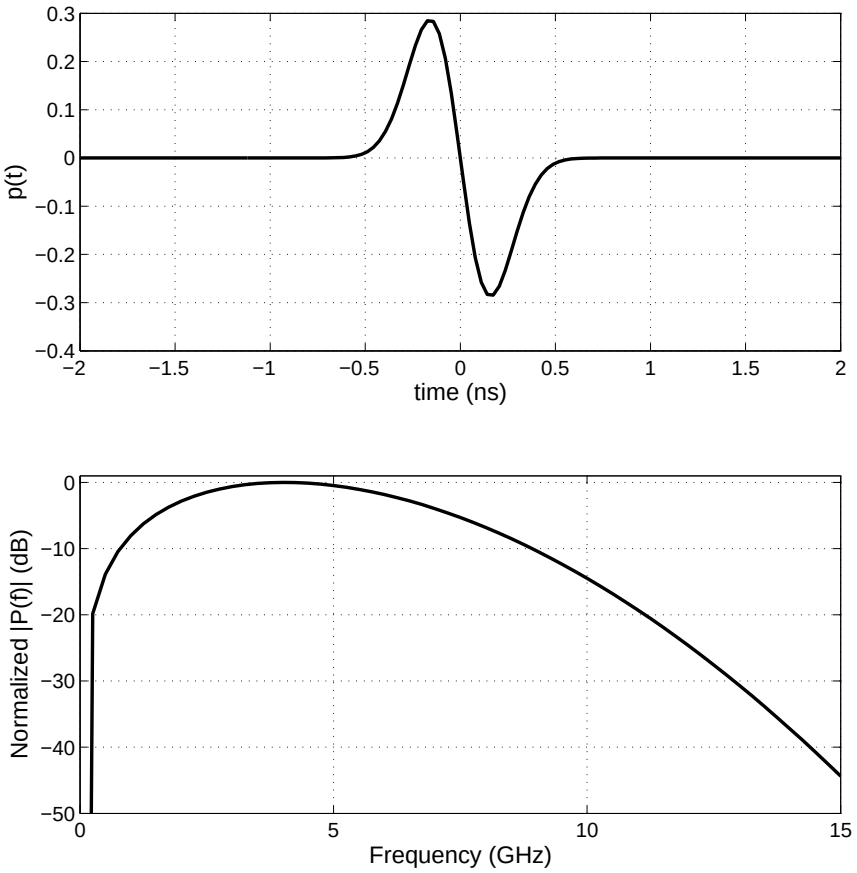

Figure 2. Time- and frequency-domain representation of 1st-order Gaussian pulse.

Modulation Index Optimization

It has been previously mentioned that the modulation index, δ, has an important role in determining the BER performance of UWB. We have demonstrated this improvement.

Without loss of generality, consider the basic Gaussian pulse function with $c = 0$,

$$p(t) = -\frac{At}{\sigma^2} e^{-\frac{t^2}{2\sigma^2}}$$

If we use $p(t)$ to represent '0' and $p(t-\delta)$ to represent '1' for binary data (see Fig. 3), the normalized correlation function of the basic pulse over a frame duration becomes (see Appendix A for detail derivation)

$$R_1(\delta) \quad = \quad \frac{1}{E_p} \int_{-\frac{T_f}{2}}^{\frac{T_f}{2}} p(t)p(t-\delta)dt,$$

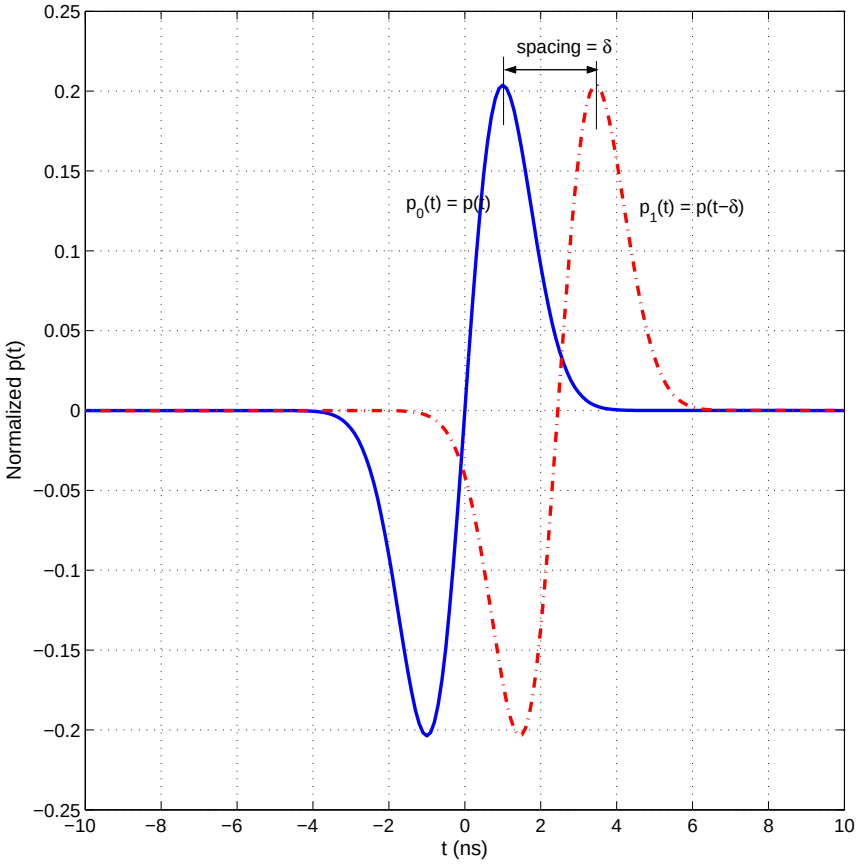

Figure 3. Pulse positioning in a binary-PPM scheme

$$\begin{aligned} &\approx \frac{1}{E_p}\int_{-\infty}^{\infty} p(t)p(t-\delta)dt \qquad (p(t)\approx 0 \text{ for } |t| \in (\tfrac{T_f}{2},\infty)) \\ &= \frac{A^2\sqrt{\pi}}{\sigma E_p}\left(0.5-\pi^2\alpha^2\right)e^{-\pi^2\alpha^2}, \end{aligned} \tag{3}$$

where $\delta = 2\pi\sigma\cdot\alpha$ has been substituted and E_p is the energy per pulse defined as:

$$E_p = \int_{-\frac{T_f}{2}}^{\frac{T_f}{2}} |p(t)|^2\, dt.$$

Assuming additive white Gaussian noise (AWGN) and single-user environment, the problem of reducing the BER (same as increasing the minimum distance between symbols) becomes the problem of finding δ that reduces the correlation in Equation (3) above. The modulation index that yields the least possible correlation is called the *optimum* modulation index, δ_{opt}. To obtain δ_{opt}, Equation (3) is differentiated

and set to zero:

$$\begin{aligned} R_1'(\delta) &= \left.\frac{dR_1(\delta)}{d\delta}\right|_{\delta=2\pi\sigma\alpha} \\ &= \frac{A^2\sqrt{\pi}}{\sigma E_p}\left(-2\pi^2\alpha\, e^{-\pi^2\alpha^2}\right)\cdot\left(\frac{3}{2}-\pi^2\alpha^2\right)=0\ . \end{aligned}$$

Further simplification shows that for the first-order Gaussian monocycle, the solution, $\alpha_{opt}=\frac{\sqrt{6}}{2\pi}$; therefore, $\delta_{opt}=\sqrt{6}\sigma\approx 0.38985(2\pi\sigma)$.

Fig. 4 shows the significance of using the optimum modulation index where the pulse width, $T_p=2\pi\sigma=1.0$ nsec, $N=1$, and $T_s=T_c=100$ nsec. As can be seen from the figure, using the optimum modulation index for the first-order Gaussian monocycle yields a 2 dB improvement compared with typically used modulation index, $\delta=0.2T_p$ [32].

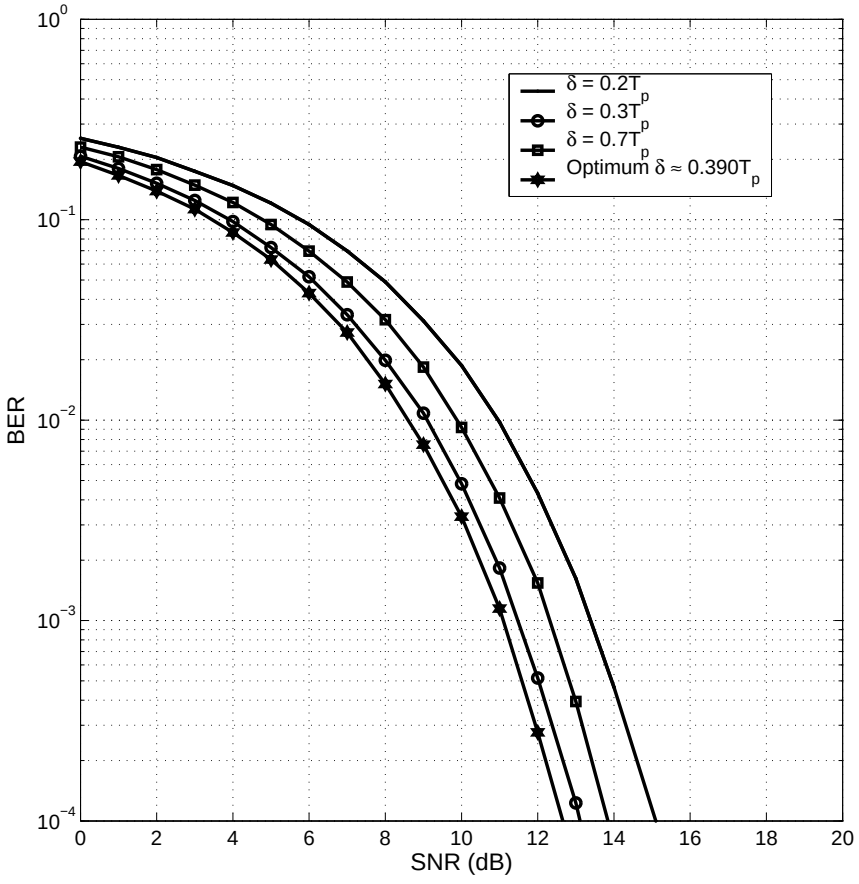

Figure 4. Performance of PPM with different modulation indexes, δ's.

The derivation above is for the first-order Gaussian monocycle. The same technique can be used on a higher order Gaussian monocycle by finding the modulation index that minimizes the normalized correlation of the k-th order Gaussian pulse, $p_k(t) = \frac{d^k}{dt^k}p(t)$, given by

$$R_k(\delta) \approx \frac{1}{E_{p_k}} \int_{-\infty}^{\infty} p_k(t)p_k(t-\delta)dt \tag{4}$$

A recursive formula can be used instead of Equation (4) to obtain the correlation formula [32]

$$R_k(\delta) = -R''_{k-1}(\delta) = (-1)^{k-1}R_1^{(2k-2)}(\delta).$$

Solving these recursive equations for the second-, third-, and fourth-order Gaussian monocycles gives the result summarized in Table 1.

Table 1. Optimum modulation indices $\delta_{opt} = 2\pi\sigma \cdot \alpha_{opt}$ and corresponding normalized correlation for various orders of Gaussian monocycle.

Pulse-order	$\alpha_{\mathbf{opt}}$	**Normalized correlation, $\mathbf{R_{min}}$**
First	$\frac{\sqrt{6}}{2\pi} \approx 0.3899$	-0.4463
Second	$\frac{\sqrt{10-2\sqrt{10}}}{2\pi} \approx 0.3051$	-0.6183
Third	0.2599	-0.7086
Fourth	0.2304	-0.7644

As seen from the table, the higher order Gaussian monocycles at their optimum modulation indexes achieve lower normalized correlation. In other words, the higher the Gaussian monocycle order, the lower the achievable BER. However, this comes at the expense of higher time-sensitivity to receiver synchronization and clock sampling jitters. This jitter sensitivity is obvious from the higher level of steepness in the correlation functions for the higher-order Gaussian monocycles as shown in Fig. 5.

Under the given optimal conditions, that is, when the modulation indexes are chosen to correspond to the point of minimum correlation values, the performance

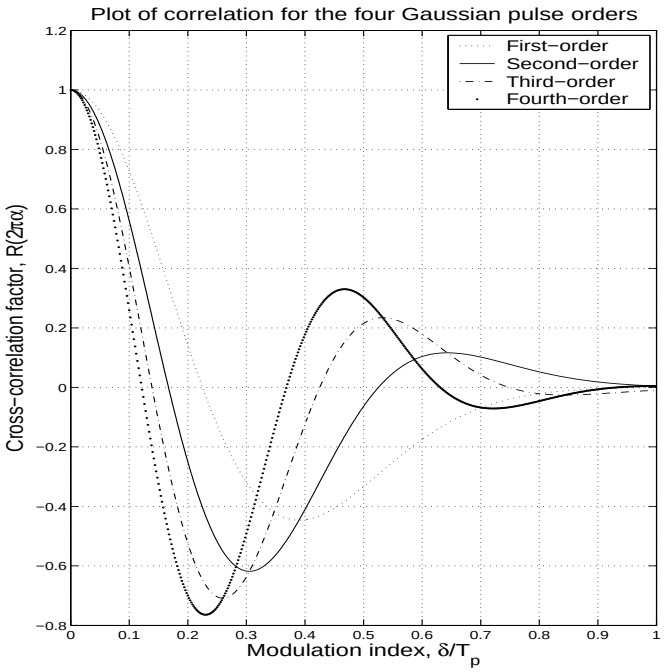

Figure 5. Correlation dependency on modulation index, δ

of the fourth-order Gaussian pulse obviously performs better than the lower orders. This is shown in Fig. 6. It is important to note that these results do not accommodate for the inevitable timing jitter that occurs at the receiver's clock sampling.

1.2.1.2 Pulse Amplitude Modulation (PAM)

PAM is another common modulation scheme used in impulse radio. For AM, the modulated signal for the m-th user in Equation (1) is replaced by:

$$s^{(m)}(t) = \sum_{n} d_n^{(m)} \cdot w^{(m)}\left(t - nT_s\right) \tag{5}$$

where

$$w^{(m)}(t) = \sum_{l=0}^{N-1} (2c_l^{(m)} - 1)p(t - nT_c),$$

and the amplitude modulating gain, $d_n^{(m)}$, can be chosen from the set $\{\pm 1, \pm 3, \cdots, \pm(2M-1)\}$ for an M-ary system, which is determined by the binary sequence, $b_n^{(m)}$, to be transmitted by user m. For example, if binary PAM is used, then $d_n^{(m)} = 2b_n^{(m)} - 1$. The primary difference between PPM and PAM is that the PPM uses the position of

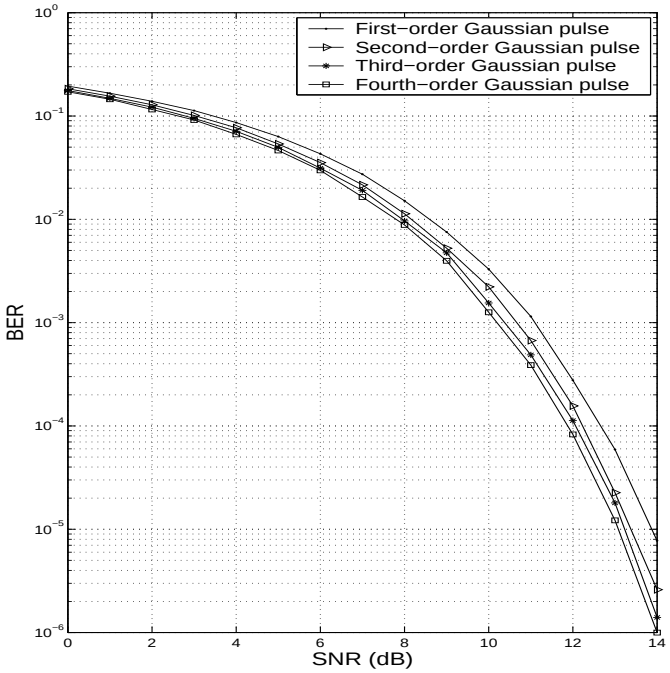

Figure 6. BER plots for the different orders of Gaussian pulse in PPM

pulse to carry information while PAM uses the pulse sign and amplitude to convey information.

1.2.1.3 **Orthogonal Pulse Modulation (OPM)**

One of the questions one may ask is why use only Gaussian monocycles for single-carrier based modulation. Is it possible to use other pulse functions to implement modulation in UWB with considerably good performance? L. Michael, M. Ghavami, and R. Kohno in [30] have used orthogonal pulses generated from Hermite polynomials as modulation pulses. In their work, a set of orthogonal pulses are used to represent the symbols for M-ary modulation; therefore, it is called *orthogonal pulse modulation* (OPM).

The Hermite polynomial is defined as,

$$f_0(t) = 1$$

$$f_n(t) = (-1)^n e^{\frac{t^2}{2}} \frac{d^n}{dt^n} \left(e^{-\frac{t^2}{2}} \right),$$

for $n = 1, 2, \cdots$. Since these polynomials are not orthogonal to each other, Gram-Schmidt procedure is used to obtain a new set of orthogonal polynomials, called *modified Hermite polynomial* (MHP) [30], which can be expressed as,

$$\begin{aligned} g_n(t) &= e^{-\frac{t^2}{4}} f_n(t) \\ &= (-1)^n e^{\frac{t^2}{4}} \frac{d^n}{dt^n} \left(e^{-\frac{t^2}{2}} \right) \end{aligned} \tag{6}$$

Using these MHPs, a multiple access scheme can be designed. Different users in the multiple access environment are assigned different pairs of polynomials for binary data transmission. Each pair, in itself, contains two orthogonal polynomials. In other words, each user uses an orthogonal pair of pulse polynomials, which are in turn orthogonal to other users' signals.

These modulation schemes described for single-carrier modulation do not form an exhaustive set of available modulations for impulse radio. These are just commonly practiced schemes. There are other single-carrier modulation schemes like On-Off Keying and orthogonal PPM for non-binary modulation.

1.2.2 Multi-carrier based

The previous section has described a few modulation schemes that are used with single-carrier UWB systems (impulse radio). In this section, we describe the multi-carrier based modulation. When dealing with multi-carrier modulation, the solution is essentially the use of *orthogonal frequency division modulation* (OFDM). One of the advantages of using this scheme is that it provides a better resistance to channel delay delay spread and a readily simple scheme for multiple access.

The OFDM technique used in UWB is fundamentally the same as in normal OFDM, which was first discussed in [41]. A baseband OFDM signal can be presented by

$$s(t) = \sum_{k=-\frac{N}{2}+1}^{\frac{N}{2}} d_k e^{j2\pi f_k t}, \tag{7}$$

for $0 \leq \mathrm{t} \leq NT_s$, where N is the number of subcarriers per OFDM block, which also equals the number of transmitted symbols per OFDM block, d_k represents the complex symbol to be transmitted and $f_k = f_0 + k\Delta f$ is the subcarrier frequency, and Δf is the frequency spacing between two adjacent subcarriers. To demodulate OFDM signals, it is required that $NT_s\Delta f = 1$, which is called the *orthogonal condition*.

When $f_o = 0$, it can be proved that the sampled version of the OFDM signal can be expressed as,

$$s(nT_s) = \sum_{k=-\frac{N}{2}+1}^{\frac{N}{2}} d_k e^{j2\pi\frac{nk}{N}}.$$

Therefore, inverse *discrete Fourier transform* (DFT) can be used to convert the transmitted symbols into OFDM signal, which has an efficient implementation - *fast Fourier transform* (FFT)

With this condition, the transmitted symbol can be detected by

$$\begin{aligned}
\frac{1}{NT_s}\int_0^{NT_s} s(t)e^{-j2\pi f_k t}dt &= \frac{1}{NT_s}\int_0^{NT_s}\left(\sum_{l=-\frac{N}{2}+1}^{\frac{N}{2}} d_l e^{j2\pi f_l t}\right)e^{-j2\pi f_k t}dt \\
&= \sum_{l=-\frac{N}{2}+1}^{\frac{N}{2}} d_l\left(\frac{1}{NT_s}\int_0^{NT_s} e^{j2\pi f_l t}e^{-j2\pi f_k t}dt\right) \\
&= \sum_{l=-\frac{N}{2}+1}^{\frac{N}{2}} d_l\delta[l-k] = d_k. \qquad (8)
\end{aligned}$$

It can be also proved that the transmitted symbols can be obtained by taking DFT to $\{s(nT_s)\}_{n=0}^{N-1}$, the T_s-sampled version of OFDM signal, $s(t)$.

In the above discussion, we have ignored channel's delay spread and noise. For UWB channels with delay spread, cyclic extension needs to be used. With proper cyclic extension, the demodulated signal can be expressed as [41]

$$\hat{r}_k = H_k d_k + n_k, \qquad (9)$$

where H_k is the UWB channel's frequency response at the k-th subcarrier, n_k represents the effect of channel noise.

CHAPTER 2

TIMING JITTER IN IMPULSE RADIO

Timing jitter results because of the presence of non-ideal sampling clocks in practical receivers. This distortion affects the correlation of signals at the receiver and thus the signal detection ability of the UWB system. The fact that impulse radio employs pulses with very narrow width (typically, less than a nanosecond) makes the sensitivity to timing jitter more significant.

2.1 Model Description

For the sake of description, we consider the first-order Gaussian monocycle previously described in Section 1.2.1,

$$p(t) = \frac{A}{\sigma}\left(c - \frac{t}{\sigma}\right) e^{-0.5\left(\frac{t}{\sigma}-c\right)^2}.$$

Suppose the sampling interval is Δ_s, then the received samples processed (ignoring the additive noise) is

$$p(n\Delta_s + \epsilon) = \frac{A}{\sigma}\left(c - \frac{n\Delta_s + \epsilon}{\sigma}\right) e^{-0.5\left(\frac{n\Delta_s+\epsilon}{\sigma}-c\right)^2},$$

where ϵ is the timing jitter and n is the sampling epoch. This timing jitter is often modeled as a *wide sense stationary* (WSS) Gaussian process with zero-mean and variance σ_J^2 [31]. As indicated in [12, 26], the *root-mean-square* (RMS) of timing jitter, σ_J, typically ranges from 10 to 150 ps in UWB receivers.

2.2 Effects of jitter on Impulse Radio

The specific effect of timing jitter on an impulse radio system depends on the modulation scheme being used. However, one underlying effect is that timing jitter distorts

the correlation property of the basis signal, thereby resulting in a term called "jitter noise". For instance, when the PPM modulation scheme is used, timing jitter distorts the correlation at the optimal modulation index. We have performed simulations to illustrate these effects for a binary PPM and a binary PAM system. The results are shown in Fig. 7 and Fig. 8.

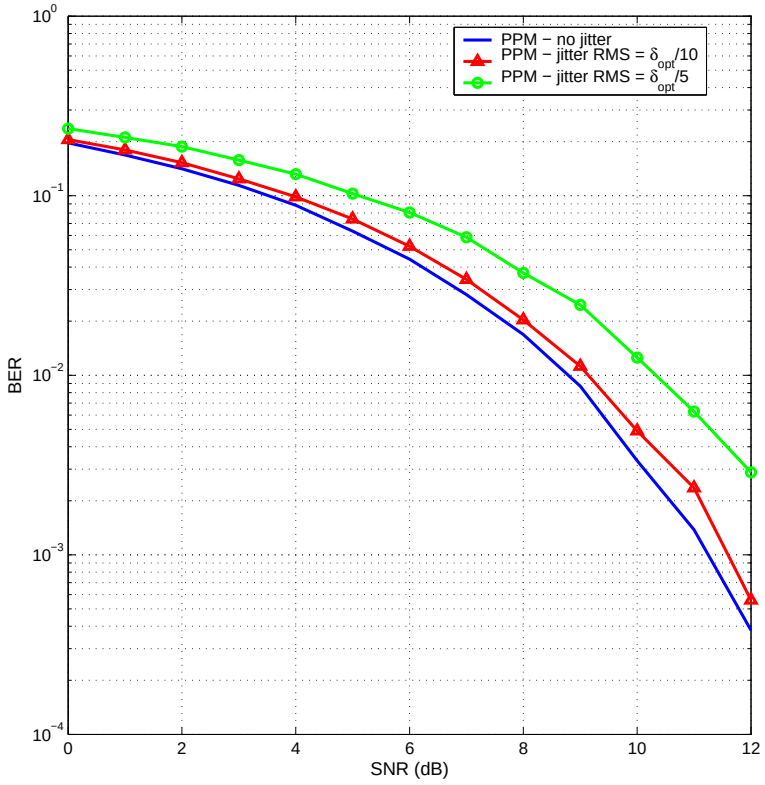

Figure 7. Effect of timing jitter on binary PPM

To maintain uniformity in the simulation, the modulation index δ_{opt} has been used as a basis for the timing jitter RMS even for the binary PAM, where δ_{opt} is not explicitly used in the basis signal equation. This simulation has been performed for a first-order Gaussian monocycle with width of 1 ns, which means a timing jitter RMS of $\delta/5$ and $\delta/10$ correspond to RMS of about 80 ps and 40 ps respectively. This shows that timing jitter RMS of 80 ps can result in a loss of up to 2 dB in SNR at a BER of 10^{-3} for both the binarry PPM and PAM.

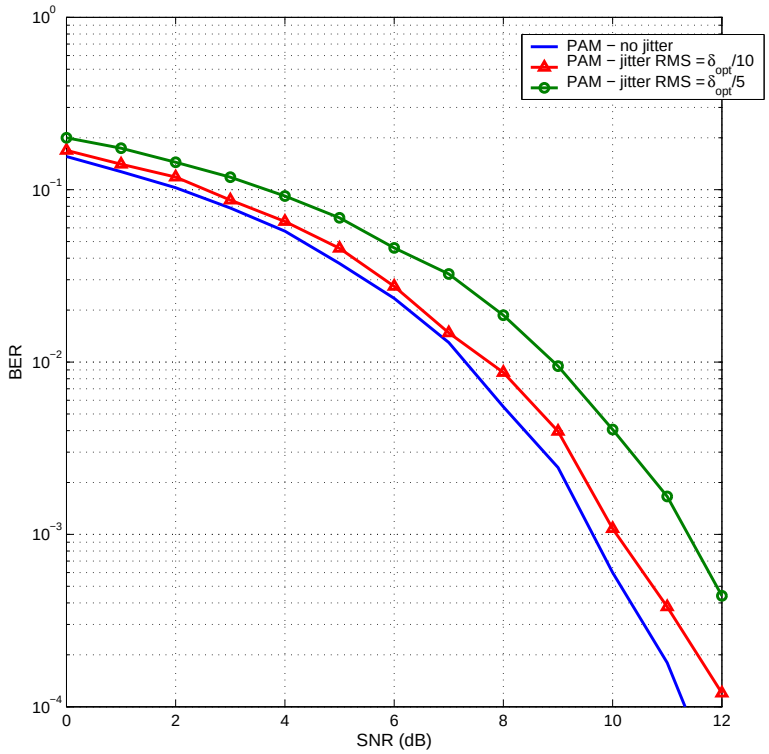

Figure 8. Effect of timing jitter on binary PAM

2.3 Reduction of jitter noise in Impulse Radio

As seen from Section 2.2, timing jitter RMS of only 80 ps for a pulse width of 1 ns, can cause serious degradation in the performance of an impulse radio system. This warrants a need to reduce the effect of jitter noise on the performance. A number of sophisticated schemes have been considered for dealing with this timing jitter effect in impulse radio [18, 19]. In this work, we propose two relatively simple but efficient schemes.

2.3.1 Pulse-shaping

Since the transmitted pulse shape determines the correlation property of the received signals, one way to reduce the effect of timing jitter is to use pulse shapes that are more resistant to jitter noise. Resistance to jitter noise is determined by the steepness exhibited around the minimum of the correlation curves (see Fig. 5). For this reason,

the Gaussian first and second-order monocycles are preferred choice over the third and fourth-order when the timing jitter RMS is significantly high. As an illustration, we performed simulation results of the BER performance of PPM using two different orders of the Gaussian monocycle with same pulse width of 1 ns. The two monocycles are

$$\begin{aligned} p_{\text{1st-Ord}}(t) &= At \exp\left(-\frac{1}{2}t^2\right) \\ p_{\text{4th-Ord}}(t) &= \mathcal{A}(t^4 - 6t^2 + 3) \exp\left(-\frac{1}{2}t^2\right) \end{aligned}$$

and the results are shown in Fig. 9. As seen, using the fourth-order Gaussian monocy-

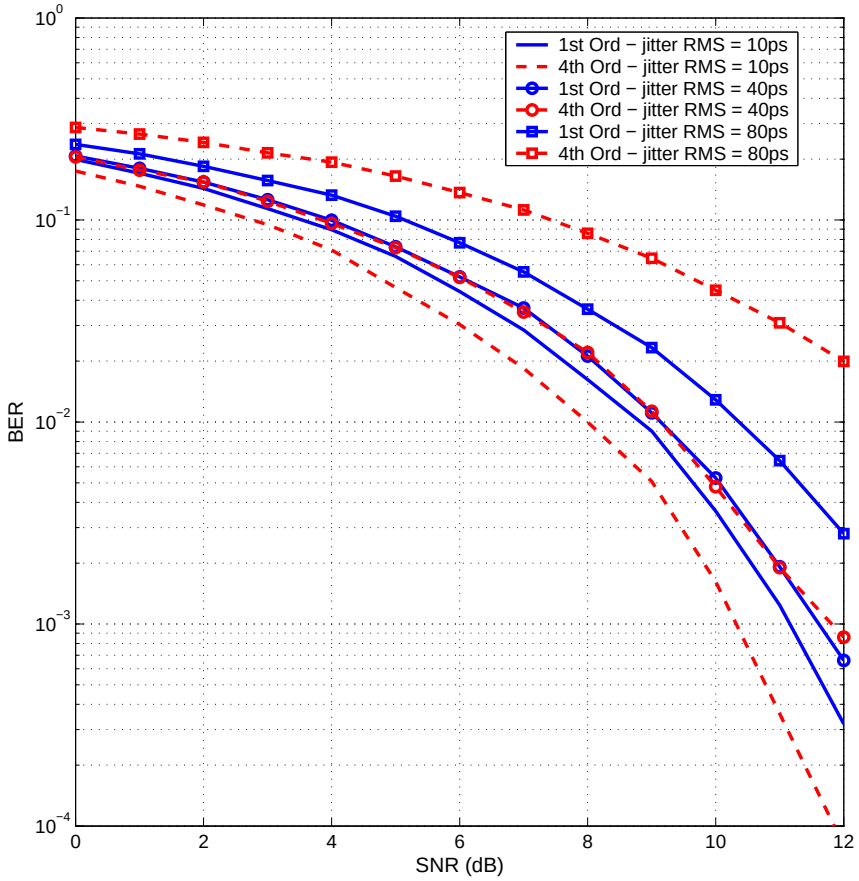

Figure 9. Pulse shaping to mitigate timing jitter in PPM (pulse width = 1 ns)

cle gives a better BER performance than its first-order counterpart when the RMS of the timing jitter is relatively small (less than 40 ps). However, when the timing jitter

RMS is considerably large, the fourth-order Gaussian monocycle deteriorates rapidly, even losing more than 5 dB in performance at BER of 10^{-2}. This is not surprising since the fourth-order, though under ideal timing conditions (no jitter) yields better performance than first-order, has a greater timing sensitivity as seen from Fig. 5. This means that other means have to be used to further reduce the effect of the jitter noise. For a simple receiver structure, employing a PPM modulation scheme for impulse radio, Fig. 9 suggests that a first-order Gaussian monocycle, $p_{\text{1st-Ord}}(t)$, makes a better choice for high timing jitter RMS sampling clocks.

We further extend the simulation to the case of binary PAM. Again, the two pulse shapes in consideration are the first-order and fourth-order Gaussian monocycle. Once again, the fourth-order Gaussian pulse experiences greater deterioration due to timing jitter. Notice that the performance of PAM using the two Gaussian pulses are about the same when there is little timing jitter. This is because the normalized correlation is -1 always for a binary PAM regardless of the pulse shape. This is different from the PPM counterpart where the fourth-order achieves a lower correlation of -0.7644 compared to -0.4463 in the first-order monocycle (see Table 1).

2.3.2 Averaging

In this scheme, we consider how averaging over a number of samples can reduce the effect of timing jitter for either a PPM or PAM using Gaussian monocycle. Without loss of generality, consider the sampled Gaussian pulse ($c \neq 0$)

$$p(t) \;=\; (1-t)e^{-\frac{c^2}{2}(1-t)^2}.$$

Then the received pulse (ignoring channel fading and noise)

$$\begin{aligned} p(n\Delta_s+\epsilon) &= (1-(n\Delta_s+\epsilon))e^{-\frac{c^2}{2}(1-(n\Delta_s+\epsilon))^2} \\ &= (1-(n\Delta_s+\epsilon))e^{-\frac{c^2}{2}(1-n\Delta_s)^2}\cdot e^{-\frac{c^2\epsilon^2}{2}}\cdot e^{c^2(1-n\Delta_s)\epsilon} \end{aligned}$$

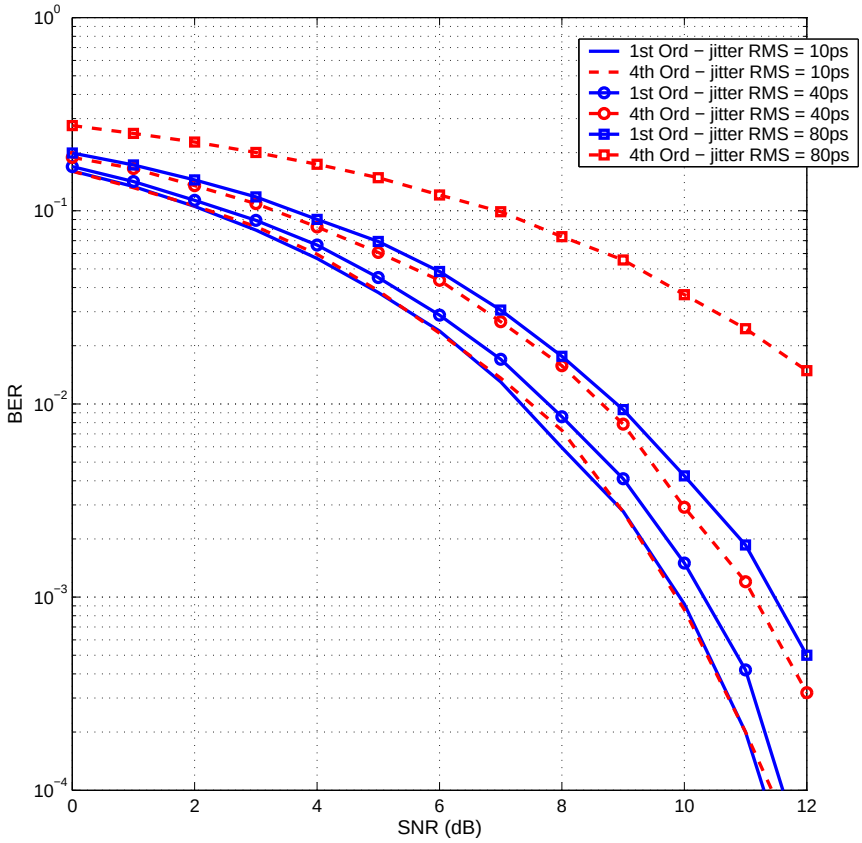

Figure 10. Pulse shaping to mitigate timing jitter in PAM (pulse width = 1 ns)

We are interested in knowing how averaging affects the pulse shape received. Notice that we have ignored the channel noise since our primary focus is on the effect of timing jitter. For analysis purposes, we assume that the timing jitter, ϵ, is a zero-mean Gaussian process. Therefore, averaging the received signal yields

$$\mathbf{E}\{p(n\Delta_s+\epsilon)\} \;=\; e^{-\frac{c^2}{2}(1-n\Delta_s)^2}\int_{-\infty}^{\infty}(1-n\Delta_s-x)e^{-\frac{c^2x^2}{2}}\cdot e^{c^2(1-n\Delta_s)x}\cdot\frac{1}{\sqrt{2\pi}}e^{-\frac{x^2}{2\sigma_\epsilon^2}}dx,$$

where σ_ϵ is the RMS of the timing jitter.

Evaluating this integral gives

$$\mathbf{E}\{p(n\Delta_s+\epsilon)\} = e^{-\frac{c^2}{2}(1-n\Delta_s)^2}\underbrace{\left(1-n\Delta_s-\frac{c^2(1-n\Delta_s)}{2\left(c^2+\frac{1}{\sigma_\epsilon^2}\right)}\right)\exp\left\{\frac{c^4(1-n\Delta_s)^2}{8\left(c^2+\frac{1}{\sigma_\epsilon^2}\right)}\right\}}_{\text{Ideally we want this to be } 1-n\Delta_s} \qquad (10)$$

It is true that this scheme does not exactly re-construct the ideal sampled pulse with no jitter, but it is still practically robust to jitter effect. To illustrate this, we consider

two extreme scenarios. First, when $\sigma_\epsilon = 0$, which means that there is no timing jitter, the term $\frac{1}{\sigma_\epsilon^2} \to \infty$ and Equation (10) becomes

$$e^{-\frac{c^2}{2}(1-n\Delta_s)^2}\left(1 - n\Delta_s - \frac{c^2(1-n\Delta_s)}{2\left(c^2+\frac{1}{\sigma_\epsilon^2}\right)}\right)\exp\left\{\frac{c^4(1-n\Delta_s)^2}{8\left(c^2+\frac{1}{\sigma_\epsilon^2}\right)}\right\} \to \underbrace{e^{-\frac{c^2}{2}(1-n\Delta_s)^2}(1-n\Delta_s)}_{p(n\Delta_s)}$$

as expected. On the other hand, if σ_ϵ is very large, that is, extreme timing jitter situation at the receiver, then $\frac{1}{\sigma_\epsilon^2} \to 0$ and we have

$$e^{-\frac{c^2}{2}(1-n\Delta_s)^2}\left(1 - n\Delta_s - \frac{c^2(1-n\Delta_s)}{2\left(c^2+\frac{1}{\sigma_\epsilon^2}\right)}\right)\exp\left\{\frac{c^4(1-n\Delta_s)^2}{8\left(c^2+\frac{1}{\sigma_\epsilon^2}\right)}\right\} \to \frac{1}{2}e^{-\frac{3c^2}{8}(1-n\Delta_s)^2}(1-n\Delta_s),$$

which in essence gives received samples whose correlation is different from the ideal but still close enough to the template transmitted signal.

Simulations were conducted to illustrate the ability of averaging in reducing the effect of timing jitter in PPM. In the simulation, the timing jitter RMS is 80 ps for a pulse width of 1 ns, and the number of measured samples used in the sample averaging is just 10. The results are shown in Fig. 11. What we notice is that at low SNR, the channel noise is dominant and hence improvement in the BER is considerably low. However, as the SNR increases, the measurements distortions are dominated by the timing jitter effect, thereby resulting in SNR gains of 0.5 dB at BER of 10^{-4} with just 10 samples averaging.

This gain in using sample averaging becomes more pronounced when we employ a fourth-order Gaussian monocycle in PPM. With the same timing jitter RMS of 80 ps and pulse width of 1 ns, the results obtained from averaging is shown in Fig. 12. As seen from the figure, the high SNR plot indicates a gain of 1.5 dB at BER of 0.004.

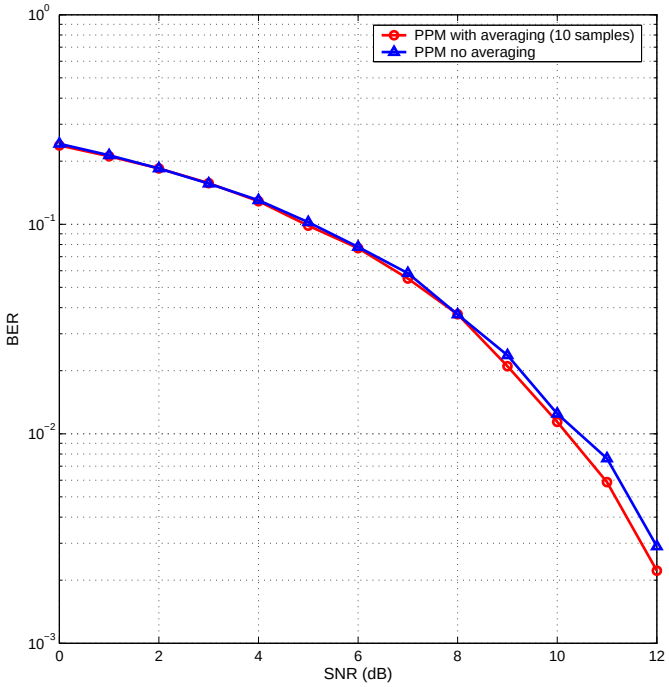

(a) low SNR

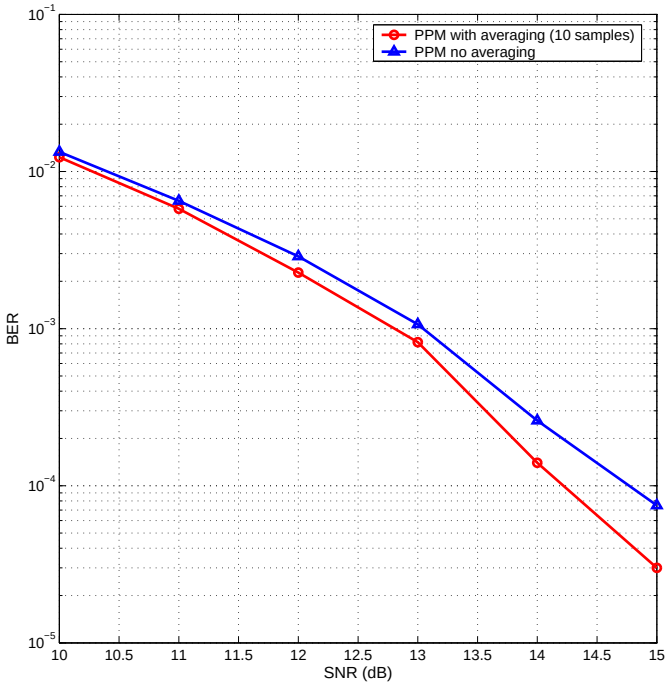

(b) high SNR

Figure 11. The effect of sample averaging on mitigating timing jitter effect for PPM (using first-order monocycle).

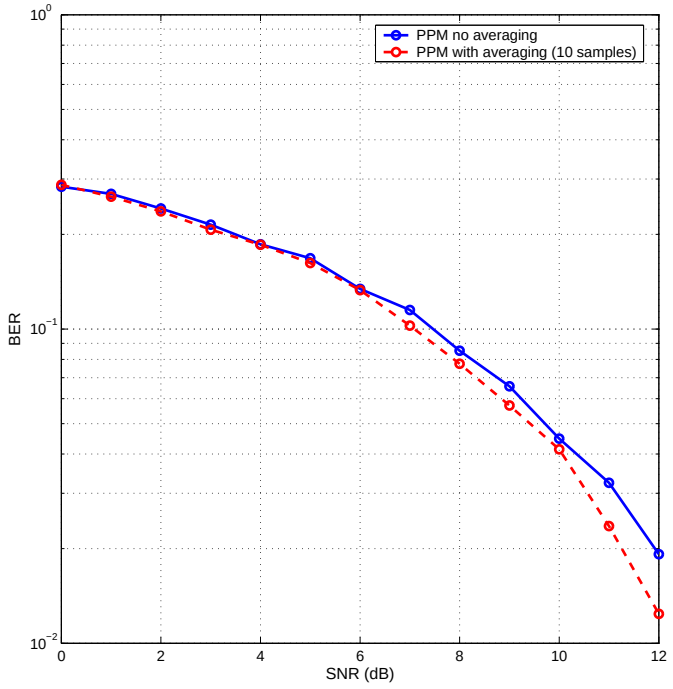

(a) low SNR

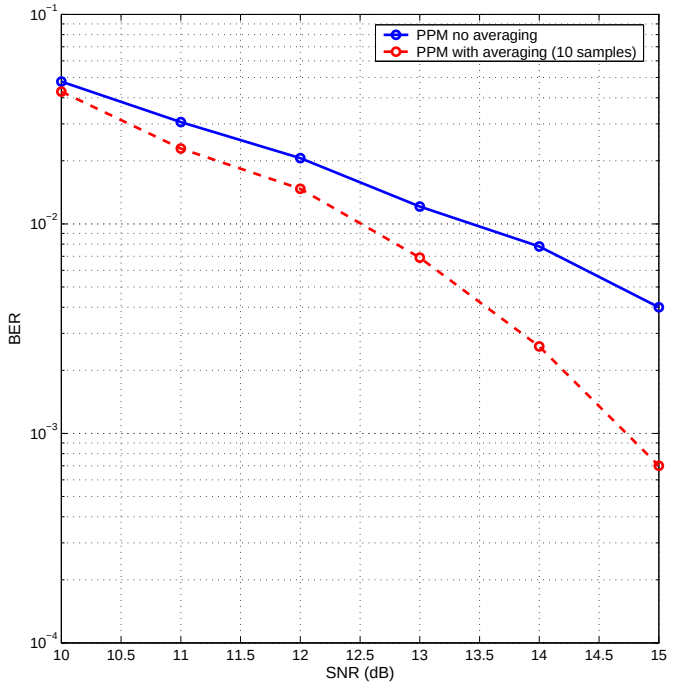

(b) high SNR

Figure 12. The effect of sample averaging on mitigating timing jitter effect for PPM (using fourth-order monocycle).

CHAPTER 3

TIMING JITTER IN OFDM-BASED UWB

Timing jitter in OFDM-based UWB systems deteriorates system performance. This is caused by the introduction of *inter-channel interference* (ICI). This chapter presents a derivatioin of the exact expression of the ICI power resulting from timing jitter and the various bounds on the ICI power. Afterwards, we will explore the ICI reduction schemes proposed in this work in Chapter 4.

3.1 Model Description

For an OFDM-based UWB, the sampled demodulated OFDM signal at the receiver is given by

$$\begin{aligned} \hat{s}_m &= \frac{1}{N} \sum_{n=-\frac{N}{2}+1}^{\frac{N}{2}} s(n\Delta t + \tau_n) e^{-j\frac{2\pi mn}{N}} \\ &= \sum_{k=-\frac{N}{2}+1}^{\frac{N}{2}} s_k \left(\frac{1}{N} \sum_{n=-\frac{N}{2}+1}^{\frac{N}{2}} e^{j\frac{2\pi}{N}(k-m)n} \cdot e^{j2\pi f_k \tau_n} \right), \end{aligned} \tag{11}$$

for $m = -\frac{N}{2} + 1, ..., \frac{N}{2}$, where τ_n is the timing jitter at the n-th sampling epoch. We conveniently leave out the additive channel noise in the analysis since it has no effect on the actual ICI power we intend to quantify (see Appendix D). The properties of the timing jitter, τ_n, are as defined earlier for impulse radio systems in Section 2.1. We have omitted the effect of fading channel and additive channel noise to simplify the analysis. To clearly show the effect of timing jitter, we break Equation (11) into two components as

$$\hat{s}_m = \eta_m \cdot s_m + \alpha_m, \tag{12}$$

where

$$\alpha_m = \sum_{k=-\frac{N}{2}+1, k\neq m}^{\frac{N}{2}} s_k \left(\frac{1}{N} \sum_{n=-\frac{N}{2}+1}^{\frac{N}{2}} e^{j\frac{2\pi}{N}(k-m)n} \cdot e^{j2\pi f_k \tau_n} \right), \tag{13}$$

is the ICI introduced by symbols at other subcarriers and

$$\eta_m = \frac{1}{N} \sum_{n=-\frac{N}{2}+1}^{\frac{N}{2}} e^{j2\pi f_m \tau_n},$$

is the gain and phase rotation of the desired symbol. As expected, if there is no timing jitter ($\tau_n = 0$), the ICI, α_m, vanishes, and the gain term η_m becomes unity.

The average ICI power on the m-th subcarrier is the expected value of the complex-valued ICI term, $\frac{1}{2}E\left|\alpha_m\right|^2$. Note that the mean of α_m is zero because the symbols, s_k's, are assumed to be zero mean. Thus, the average ICI power is

$$\begin{aligned}
P_{ICI}(m) &= \frac{1}{2}E\left\{|\alpha_m|^2\right\} \\
&= \frac{1}{2}E\left\{ \left| \sum_{k=-\frac{N}{2}+1, k\neq m}^{\frac{N}{2}} s_k \left(\frac{1}{N} \sum_{n=-\frac{N}{2}+1}^{\frac{N}{2}} e^{j\frac{2\pi}{N}(k-m)n} \cdot e^{j2\pi f_k \tau_n} \right) \right|^2 \right\} \\
&= \frac{1}{2}E\left\{ \frac{1}{N^2} \sum_{k\neq m} \sum_{l\neq m} \sum_{n=-\frac{N}{2}+1}^{\frac{N}{2}} \sum_{p=-\frac{N}{2}+1}^{\frac{N}{2}} s_k s_l^* e^{j2\pi(f_k\tau_n - f_l\tau_p)} \cdot e^{j\frac{2\pi}{N}[(k-m)n-(l-m)p]} \right\} \\
&= \frac{1}{N^2} \sum_{k\neq m} \sum_{l\neq m} \sum_{n=-\frac{N}{2}+1}^{\frac{N}{2}} \sum_{p=-\frac{N}{2}+1}^{\frac{N}{2}} \frac{1}{2}E\{s_k s_l^*\} \cdot E\left\{e^{j2\pi(f_k\tau_n - f_l\tau_p)}\right\} \times \\
&\quad e^{j\frac{2\pi}{N}[(k-m)n-(l-m)p]} \\
&= \frac{\sigma_s^2}{N^2} \sum_{k\neq m} \sum_{n=-\frac{N}{2}+1}^{\frac{N}{2}} \sum_{p=-\frac{N}{2}+1}^{\frac{N}{2}} E\left\{e^{j2\pi f_k(\tau_n - \tau_p)}\right\} e^{j\frac{2\pi}{N}(k-m)(n-p)}.
\end{aligned}$$

When timing jitters $\{\tau_n\}$ are WSS Gaussian, the expectation in the summation will be

$$P_{ICI}(m) = \frac{\sigma_s^2}{N^2} \sum_{k\neq m} \sum_{n=-\frac{N}{2}+1}^{\frac{N}{2}} \sum_{p=-\frac{N}{2}+1}^{\frac{N}{2}} e^{-4\pi^2 f_k^2 \sigma_J^2 (1-\rho_{n-p})} e^{j\frac{2\pi}{N}(k-m)(n-p)}. \tag{14}$$

From the above formula, we proceed to obtain the exact ICI power resulting from

timing jitter in OFDM-based UWB. From the exact ICI power, we will derive the bounds on the ICI power for white and colored timing jitter.

3.2 ICI resulting from timing jitter

Timing jitter can be studied in one of two forms - as correlated (colored timing jitter) or uncorrelated (white timing jitter). From a real system standpoint, when the sampling rate increases, the timing jitters at adjacent clock samples become more correlated. However, there is no exact model to describe the correlation of timing jitters yet. To analyze the impact of colored timing jitter on OFDM based UWB systems, we assume that the correlation function is either Gaussian-shaped or exponential. Similar assumption has been made in [3, 31], where the correlation model given is equivalent to the exponential correlation described below.

The correlation coefficient between timing jitters at two samples separated by t can be expressed as

$$\rho(t) = e^{-\beta^2 t^2}, \tag{15}$$

for the Gaussian correlation and

$$\rho(t) = e^{-a|t|}, \tag{16}$$

for the exponential correlation, where β and a are positive parameters that describe level of correlation. The smaller the β or a, the larger is the correlation.

If the sampling interval is $\Delta t = T_s/N$, then the correlation coefficient between τ_n and τ_l, the timing jitters at the samples at times $n\Delta t$ and $l\Delta t$ (n-th and l-th samples), respectively, will be

$$\rho_{n-l} = \rho(n\Delta t - l\Delta t).$$

For example, for the Gaussian correlation,

$$\rho_{n-l} = e^{-\alpha^2 (n-l)^2}, \tag{17}$$

where $\alpha = \beta\Delta t$.

3.2.1 ICI Resulting from white timing jitter

When timing jitter is white, the correlation coefficient is

$$\rho_m = \begin{cases} 1, & \text{when } m = 0, \\ 0, & \text{when } m \neq 0. \end{cases}$$

Then, the average ICI power can be expressed as

$$\begin{aligned} P_{ICI}(m) &= \underbrace{\frac{\sigma_s^2}{N^2} \sum_{k \neq m} \sum_{n=-\frac{N}{2}+1}^{\frac{N}{2}} \sum_{p=-\frac{N}{2}+1}^{\frac{N}{2}} e^{-4\pi^2 f_k^2 \sigma_J^2} e^{j\frac{2\pi}{N}(k-m)(n-p)}}_{=\ 0} \\ &\quad + \underbrace{\frac{\sigma_s^2}{N^2} \sum_{k \neq m} \sum_{n=-\frac{N}{2}+1}^{\frac{N}{2}} \sum_{p=-\frac{N}{2}+1}^{\frac{N}{2}} \left(1 - e^{-4\pi^2 f_k^2 \sigma_J^2}\right) \delta[n-p] e^{j\frac{2\pi}{N}(k-m)(n-p)}}_{\neq\ 0} \\ &= \frac{\sigma_s^2}{N^2} \sum_{k \neq m} \left(1 - e^{-4\pi^2 f_k^2 \sigma_J^2}\right) \sum_{n=-\frac{N}{2}+1}^{\frac{N}{2}} \sum_{p=-\frac{N}{2}+1}^{\frac{N}{2}} \delta[n-p] e^{j\frac{2\pi}{N}(k-m)(n-p)} \\ &= \frac{\sigma_s^2}{N^2} \sum_{k \neq m} \left(1 - e^{-4\pi^2 f_k^2 \sigma_J^2}\right) \underbrace{\sum_{n=-\frac{N}{2}+1}^{\frac{N}{2}} e^{j\frac{2\pi}{N}(k-m)\cdot 0}}_{=\ N} \\ &= \frac{\sigma_s^2}{N} \sum_{k \neq m} \left(1 - e^{-4\pi^2 f_k^2 \sigma_J^2}\right) \\ &= \frac{\sigma_s^2}{N} \sum_{k \neq m} \left(1 - e^{-4\pi^2 k^2 (\Delta f)^2 \sigma_J^2}\right) \\ &= \frac{\sigma_s^2}{N} \sum_{k \neq m} \left(1 - e^{-4\pi^2 B^2 \sigma_J^2 \left(\frac{k}{N}\right)^2}\right). \end{aligned} \tag{18}$$

For an OFDM signal with a large number of subcarriers, N,

$$P_{ICI} = \sigma_s^2 \int_{-\frac{1}{2}}^{\frac{1}{2}} \left(1 - e^{-4\pi^2 (B\sigma_J)^2 x^2}\right) dx. \tag{19}$$

This result shows that the ICI power is virtually determined by the bandwidth-RMS timing jitter product, $B\sigma_J$.

To obtain upper and lower bounds, we use the following inequalities,

$$1 - x^2 \leq e^{-x^2} \leq 1 - x^2 + \frac{x^4}{2}$$

or

$$x^2 - \frac{x^4}{2} \leq 1 - e^{-x^2} \leq x^2$$

for $x^2 < 1$. In practical OFDM-based UWB systems, the product $B\sigma_J \ll 1$ (typical values are $B = 500$ MHz, and $\sigma_J = 100$ ps, which yields $B\sigma_J = 0.05 \ll 1$), so we can apply the above inequalities to Equation (19) to give

$$\sigma_s^2 \int_{-\frac{1}{2}}^{\frac{1}{2}} \left(4\pi^2 (B\sigma_J)^2 x^2 - 8\pi^4 (B\sigma_J)^4 x^4\right) dx \;\; \leq P_{ICI} \leq \;\; \sigma_s^2 \int_{-\frac{1}{2}}^{\frac{1}{2}} 4\pi^2 (B\sigma_J)^2 x^2 dx.$$

Consequently,

$$\frac{\pi^2 (B\sigma_J)^2}{3}\left[1 - \frac{3\pi^2 (B\sigma_J)^2}{10}\right] \;\; \leq \frac{P_{ICI}}{\sigma_s^2} \leq \;\; \frac{\pi^2}{3}(B\sigma_J)^2. \tag{20}$$

Our previous works confirm the accuracy of the derived bounds and quantify the impact of white timing jitter using the numerical example presented here.

Figures 13 and 14 demonstrate the ICI power for an OFDM-based UWB system with white timing jitter. The OFDM signal is assumed to have 128 subcarriers ($N = 128$). Figure 13 shows that the ICI power under white timing jitter is virtually constant at different subcarriers. Hence, the behavior of the ICI power is dictated by the $B\sigma_J$ product. This is not the case for colored timing jitter, as will be shown later.

Figure 14 compares the bounds and the exact ICI power on the subcarrier, $m = 0$, though the ICI power plot is independent of subcarrier index. From the figure, the developed bounds are seen to be very tight over a wide range of bandwidth and RMS timing jitter products. For a typical OFDM-based UWB systems, the bandwidth, B, is 500 MHz; the average ICI power ranges from -28 dB to -19 dB when the RMS of timing jitter ranges from 50 ps to 150 ps.

3.2.2 ICI Resulting from colored timing jitter

Timing jitters at adjacent symbols may be correlated when the sampling interval is small enough. In this section, we will discuss the ICI power resulting from colored

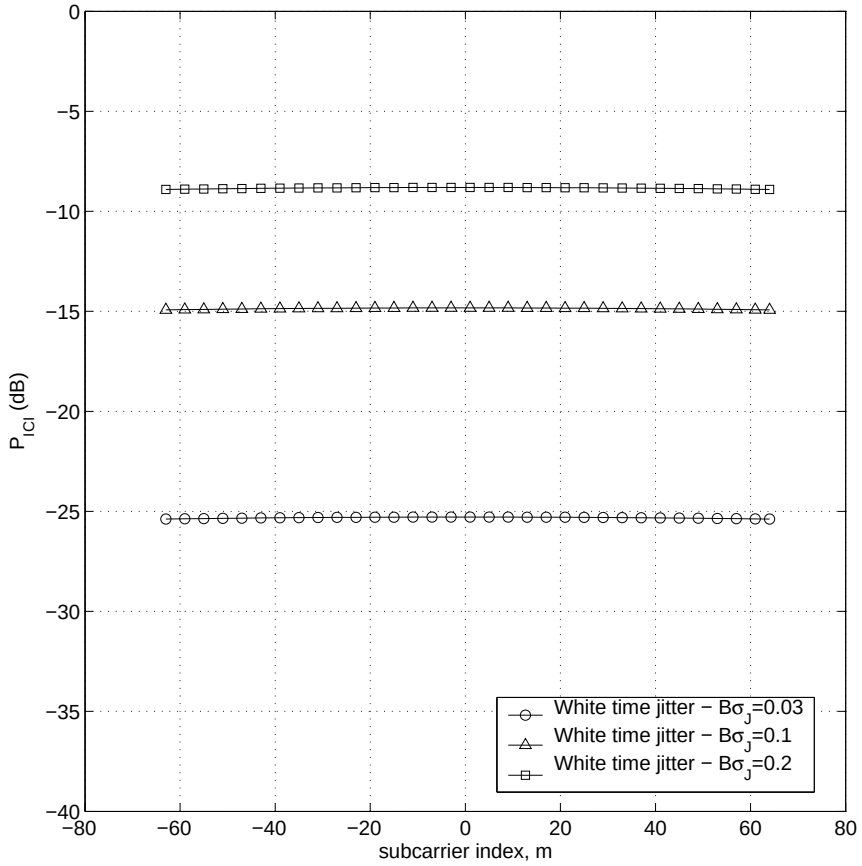

Figure 13. Variation of the ICI power with the subcarrier index, m, for a system with white timing jitter, $N = 128$.

timing jitters. It will be seen that the ICI power is subcarrier dependent, which is different from the case of white timing jitter. Therefore, finding a simple ICI power bound for all subcarriers is in general very difficult. As such, we only derive a universal upper bound on the ICI power.

As before, assuming $4\pi^2 B^2 \sigma_J^2 \ll 1$, we have

$$e^{-4\pi^2 f_k^2 \sigma_J^2 (1-\rho_{n-p})} \approx 1 - 4\pi^2 f_k^2 \sigma_J^2 (1 - \rho_{n-p})$$

Therefore, from Equation (14), we can re-write the ICI power as

$$\begin{aligned} P_{ICI}(m) &= \frac{\sigma_s^2}{N^2} \sum_{k \neq m} \sum_{n=-\frac{N}{2}+1}^{\frac{N}{2}} \sum_{p=-\frac{N}{2}+1}^{\frac{N}{2}} \left[1 - 4\pi^2 f_k^2 \sigma_J^2 (1 - \rho_{n-p})\right] e^{j\frac{2\pi}{N}(k-m)(n-p)} \\ &= \frac{\sigma_s^2}{N^2} \sum_{k \neq m} \sum_{l=-N+1}^{N-1} (N - |l|) \left[1 - 4\pi^2 f_k^2 \sigma_J^2 (1 - \rho_l)\right] e^{j\frac{2\pi}{N}(k-m)l} \end{aligned} \tag{21}$$

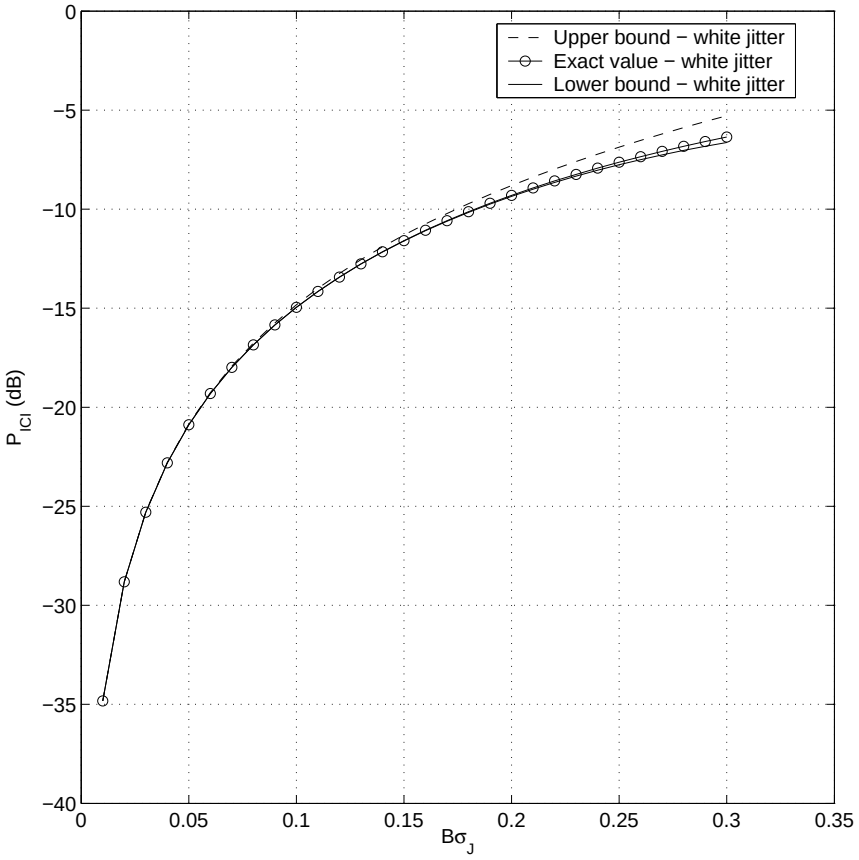

Figure 14. Comparison of the bounds and the exact ICI power for a system with white timing jitter.

It is proved in Appendix B that

$$\frac{P_{ICI}(m)}{\sigma_s^2} \approx \frac{\pi^2}{3}(B\sigma_J)^2 \left[1 + \frac{12}{N^3}\sum_{l=1}^{N-1}(-1)^l l \rho_{N-l} \frac{\cos\left(\pi \frac{l}{N} 2m\right)}{\sin^2\left(\pi \frac{l}{N}\right)}\right]. \tag{22}$$

For white timing jitter, $\rho_l = 0$ for $l \neq 0$, the ICI power is virtually subcarrier independent from the above formula. However, for colored timing jitter, $\rho_l \neq 0$ for all $l \neq 0$; therefore, the ICI power is in general subcarrier-dependent.

It can be easily shown that the average of the ICI power over all subcarriers will be

$$\frac{\bar{P}_{ICI}}{\sigma_s^2} = \frac{1}{N}\sum_{m=-\frac{N}{2}+1}^{\frac{N}{2}} \frac{P_{ICI}(m)}{\sigma_s^2} = \frac{1}{3}\pi^2(B\sigma_J)^2,$$

which is independent of the correlation coefficients of the timing jitters. Therefore, the correlation between timing jitters does not change the overall ICI power. It only

re-assigns the ICI power among different subcarriers. This is true in general when the number of subcarriers is large enough. However, when the number of subcarriers is small (typically $N \leq 32$), then a more accurate representation of the average ICI power is (see Appendix C)

$$\frac{\bar{P}_{ICI}}{\sigma_s^2} = \frac{1}{3}\pi^2(B\sigma_J)^2\left[1 - \frac{2}{N^2}\sum_{l=1}^{N-1} l\rho_{N-l}\left(1 + \frac{1}{N^2}\right)\right] \quad (23)$$

3.3 Universal Upper Bound on timing jitter induced ICI

We can obtain a universal upper bound on the ICI power resulting from colored timing jitter, which provides more insight into the worst case performance.

From (22),

$$\begin{aligned}\frac{P_{ICI}(m)}{\sigma_s^2} &\leq \frac{\pi^2}{3}(B\sigma_J)^2\left[1 + \frac{12}{N^3}\sum_{l=1}^{N-1} l|\rho_{N-l}|\frac{\left|\cos\left(\pi\frac{l}{N}2m\right)\right|}{\left|\sin^2\left(\pi\frac{l}{N}\right)\right|}\right] \\ &\leq \frac{\pi^2}{3}(B\sigma_J)^2\left[1 + \frac{12}{N^3}\sum_{l=1}^{N-1} l|\rho_{N-l}|\frac{1}{\left|\sin^2\left(\pi\frac{1}{N}\right)\right|}\right] \\ &\approx \frac{\pi^2}{3}(B\sigma_J)^2\left[1 + \frac{12}{\pi^2 N}\sum_{l=1}^{N-1} l|\rho_{N-l}|\right]. \quad (24)\end{aligned}$$

Equation (24) gives a universal upper bound on the ICI power resulting from colored timing jitter.

Figure 15 shows variation of the ICI power versus subcarrier index with bandwidth $B = 500$ MHz and number of subcarriers $N = 128$. From the figure, we note that the ICI power for colored timing jitter *does* depend on the subcarrier index. Comparing Fig. 15 (a) and Fig. 15 (b), we can see that the larger the correlation (the smaller the α), the larger the ICI power variation. In particular, when $\alpha = 0.4$, the ICI power increases from -35 dB at $m = 0$ to -22 dB at $m = N/2 = 64$. Figure 16 demonstrates the robustness of the universal upper bound on the ICI power. From the figure, the universal upper bound is very close to the ICI power of the worst subcarrier ($m = N/2 = 64$). With Gaussian correlated timing jitter, as α increases,

the timing jitter *whitens* and the ICI powers at different subcarriers tend to be the same as those of white timing jitter, as shown in Fig. 17.

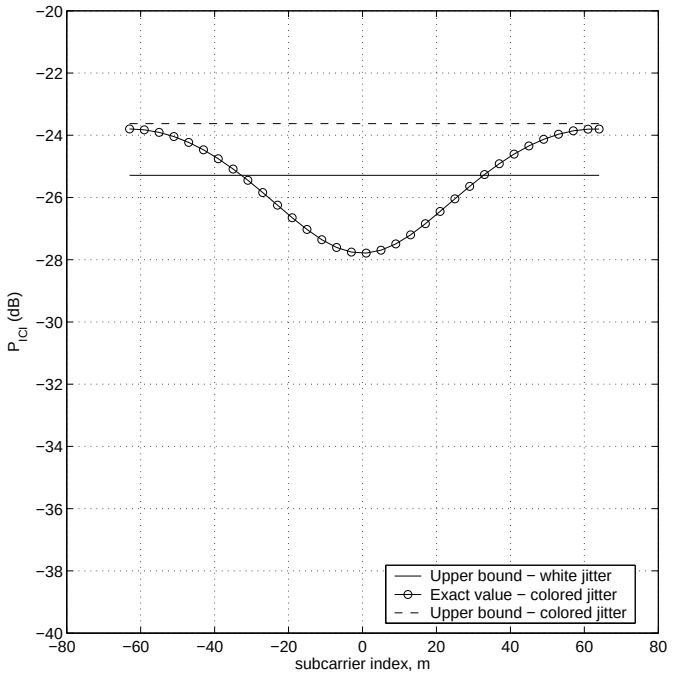

(a) $\alpha = 1$

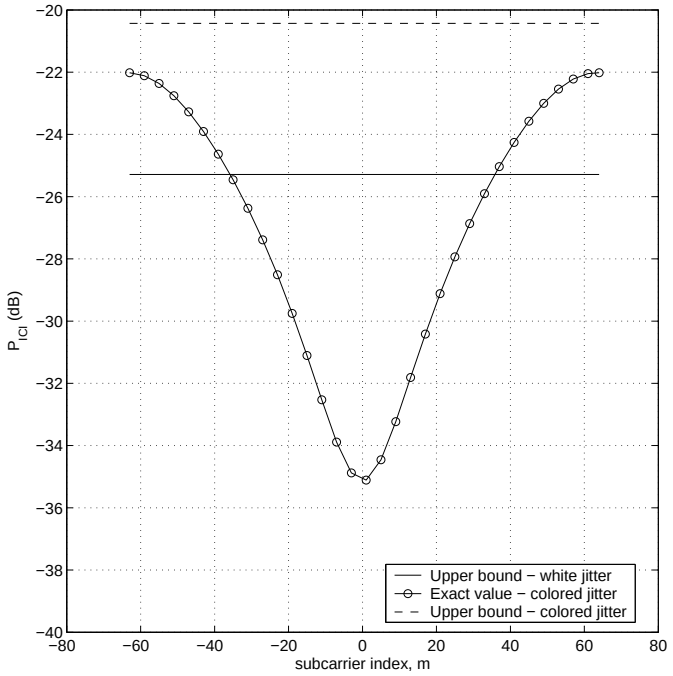

(b) $\alpha = 0.4$

Figure 15. Variation of ICI power versus subcarrier index, m, with $B\sigma_J = 0.03$ for a system with colored timing jitter.

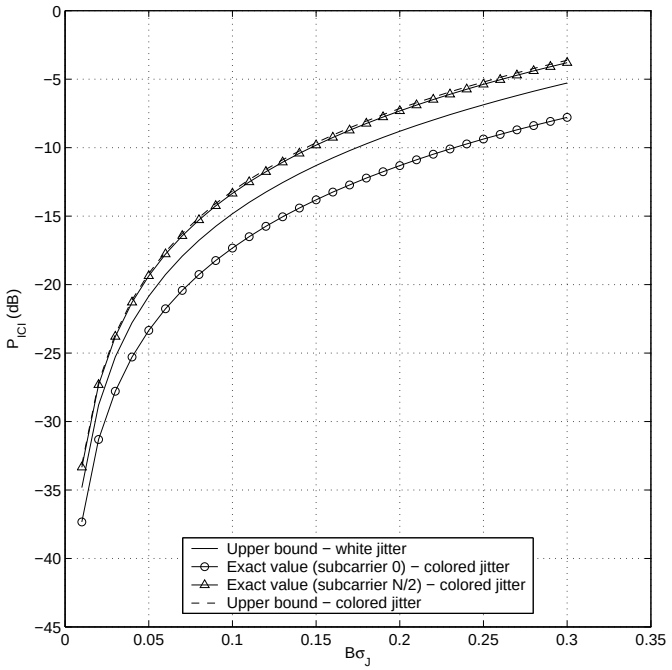

(a) $\alpha = 1$

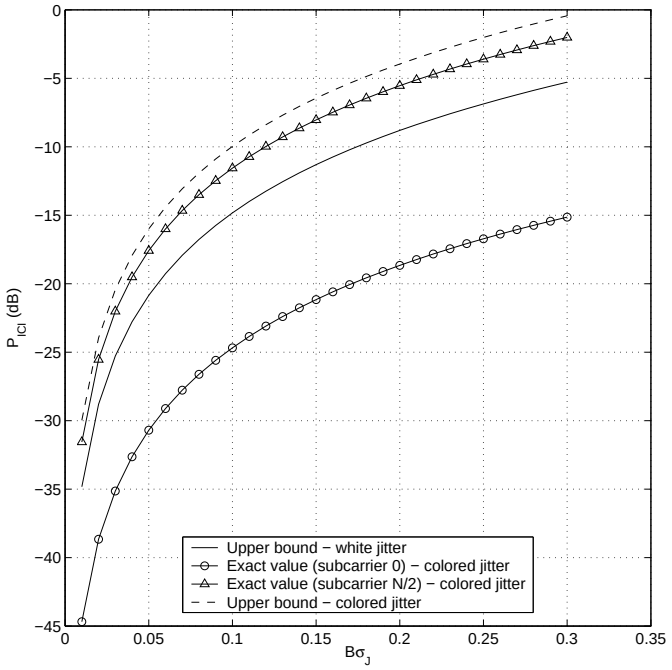

(b) $\alpha = 0.4$

Figure 16. The ICI power versus the product of bandwidth and RMS timing jitter for a system with colored timing jitter.

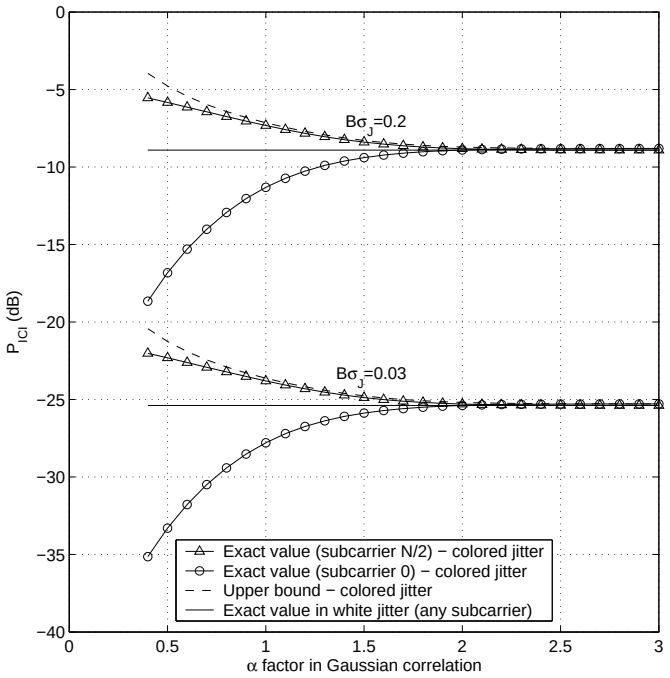

Figure 17. Variation of ICI power versus decay factor α in Gaussian correlation.

CHAPTER 4

ICI REDUCTION IN OFDM-BASED UWB

From the previous section, reducing the ICI power resulting from timing jitter can be accomplished by either reducing the bandwidth or improving sampling accuracy. However, QoS and hardware restriction normally give no room for adjusting the above parameters. When neither of those system parameters can be changed directly, we propose reducing the ICI power by either oversampling at the analog-to-digital converter of the UWB receiver, as indicated in [29], or by using adaptive modulation at the transmitter.

4.1 Oversampling

This section describes how oversampling at the receiver can mitigate of ICI for OFDM-based UWB systems.

4.1.1 ICI Power Reduction

Here we analyze the ICI power reduction by means of oversampling. Assume that we oversample OFDM signal by a factor of M. Then, the sampling time interval will be $\frac{\Delta t}{M}$ and the demodulated sequence in Equation (11) becomes

$$\begin{aligned}
\hat{s}_m^o &= \frac{1}{MN} \sum_{n=-NM/2+1}^{NM/2} s(\frac{n\Delta t}{M} + \tau_n) e^{-j\frac{2\pi mn}{MN}} \\
&= \frac{1}{MN} \sum_{k=-N/2+1}^{N/2} s_k \sum_{n=-NM/2+1}^{NM/2} e^{j2\pi\frac{n}{MN}(k-m)} e^{j2\pi f_k \tau_n} \\
&= \eta_m^o \cdot s_m + \alpha_m^o
\end{aligned}$$

where

$$\alpha_m^o = \sum_{k=-\frac{N}{2}+1, k\neq m}^{\frac{N}{2}} s_k \left(\frac{1}{MN} \sum_{n=-\frac{MN}{2}+1}^{\frac{MN}{2}} e^{j\frac{2\pi}{MN}(k-m)n} \cdot e^{j2\pi f_k \tau_n} \right)$$

and

$$\eta_m^o = \frac{1}{MN} \sum_{n=-\frac{MN}{2}+1}^{\frac{MN}{2}} e^{j2\pi f_m \tau_n}.$$

Similar to the derivation in the previous sections, the ICI power can be expressed as

$$\begin{aligned} P_{ICI}^o(m) &= \frac{1}{2} E\left|\alpha_m^o\right|^2 \\ &\approx \frac{1}{M}\frac{\pi^2}{3}(B\sigma_J)^2\sigma_s^2 + \frac{8\pi^2(B\sigma_J)^2\sigma_s^2}{(MN)^2} \times \\ &\quad \sum_{l=1}^{MN-1} l\rho((MN-l)\frac{\Delta t}{M}) \sum_{k=-\frac{N}{2}+1, k\neq m}^{\frac{N}{2}} \left(\frac{k}{N}\right)^2 \cos\left(2\pi\frac{l}{MN}(k-m)\right), \end{aligned}$$

which when divided by the average ICI power over all m, $\bar{P}_{ICI} = \frac{\pi^2}{3}(B\sigma_J)^2\sigma_s^2$, results in

$$\begin{aligned} \frac{P_{ICI}^o(m)}{\bar{P}_{ICI}} =& \frac{1}{M} + \frac{24}{(MN)^2} \times \\ & \sum_{l=1}^{MN-1} l\rho((MN-l)\frac{\Delta t}{M}) \sum_{k=-\frac{N}{2}+1, k\neq m}^{\frac{N}{2}} \left(\frac{k}{N}\right)^2 \cos\left(2\pi\frac{l}{MN}(k-m)\right). \quad (25) \end{aligned}$$

If the timing jitter is uncorrelated, that is, $\rho(l\frac{\Delta t}{M}) = 0$ for $l \neq 0$, then the second term in (25) will be zero and the ICI power will be

$$P_{ICI}^o(m) = \frac{1}{M}\bar{P}_{ICI}.$$

Therefore, oversampling by a factor of M results in a reduction of the ICI power by the same factor for the case of white timing jitter.

4.1.2 Limits of Performance Improvement

With the increase of the sampling rate, the timing jitters at adjacent samples become more and more correlated. To study the limit in performance improvement resulting from oversampling, we assume the oversampling factor, M, to be very large. In this case, we rewrite the expression of the ICI power in Equation (25) as

$$\begin{aligned} \frac{P_{ICI}^o(m)}{\bar{P}_{ICI}} &= \frac{1}{M} + \frac{24}{MN} \times \\ & \sum_{k=-\frac{N}{2}+1, k\neq m}^{\frac{N}{2}} \left(\frac{k}{N}\right)^2 \sum_{l=1}^{MN-1} (1-\frac{l}{MN})\rho(\frac{l}{MN}N\Delta t)\cos\left(2\pi\frac{l}{MN}(k-m)\right). \end{aligned}$$

As the oversampling factor, M, becomes very large, the first term tends to zero in the above expression; we can replace the second summation by an integral by taking $1/MN$ to be dx. Consequently,

$$\begin{aligned}
\frac{P^o_{ICI}(m)}{\bar{P}_{ICI}} &= 24 \sum_{k=-\frac{N}{2}+1, k\neq m}^{\frac{N}{2}} \left(\frac{k}{N}\right)^2 \int_{0^+}^{1} (1-x)\rho(x \cdot N\Delta t)\cos\left(2\pi(k-m)x\right) dx \\
&= \frac{24}{N\Delta t} \sum_{k=-\frac{N}{2}+1, k\neq m}^{\frac{N}{2}} \left(\frac{k}{N}\right)^2 \int_{0^+}^{N\Delta t} (1-\frac{x}{N\Delta t})\rho(x)\cos\left(\frac{2\pi(k-m)}{N\Delta t}x\right) dx \\
&= \frac{24B}{N} \sum_{k=-\frac{N}{2}+1, k\neq m}^{\frac{N}{2}} \left(\frac{k}{N}\right)^2 \left\{\frac{1}{2} S_\tau\left(2\pi\left(\frac{k}{N}-\frac{m}{N}\right)B\right)\right. \\
&\qquad \left. -\frac{1}{N\Delta t}\frac{1}{2} Q_\tau\left(2\pi\left(\frac{k}{N}-\frac{m}{N}\right)B\right)\right\},
\end{aligned}$$

where

$$S_\tau(\omega) = 2\int_{0^+}^{\infty} \rho(x)\cos(\omega x)dx,$$
$$Q_\tau(\omega) = 2\int_{0^+}^{\infty} x\rho(x)\cos(\omega x)dx,$$

and $B = \frac{1}{\Delta t}$.

For a large N, we can approximate the summation over k with an integral,

$$\frac{P^o_{ICI}(m)}{\bar{P}_{ICI}} \approx 12B\left\{\int_{-\frac{1}{2}}^{\frac{1}{2}} y^2 S_\tau(2\pi(y-\varepsilon_m)B)dy - \frac{B}{N}\int_{-\frac{1}{2}}^{\frac{1}{2}} y^2 Q_\tau(2\pi(y-\varepsilon_m)B)dy\right\} \quad (26)$$

where $\varepsilon_m = \frac{m}{N}$. The expression in Equation (26) does not in general equal zero unless the timing jitter process is uncorrelated, in which case both $S_\tau(\omega)$ and $Q_\tau(\omega)$ are equal to zero. Therefore, as long as the timing jitter process is correlated, a residual term could still be left in the ICI power even when the oversampling factor is very large.

4.1.3 Simulation Results

To illustrate the effect of oversampling on the ICI power and demonstrate the residue as the oversampling factor becomes very large, we use numerical examples involving

the two different correlation functions described in Section 3.2. For the Gaussian correlation function,

$$S_\tau(\omega) = \frac{\sqrt{\pi}}{\beta} e^{-\frac{\omega^2}{4\beta^2}},$$

and

$$Q_\tau(\omega) = \frac{1}{\beta^2}\left[1 + \sum_{k=1}^{\infty} \frac{1}{(2k-1)!!}\left(-\frac{\omega^2}{2\beta^2}\right)^k\right].$$

For the exponential correlation function,

$$S_\tau(\omega) = \frac{2a}{a^2+\omega^2},$$

and

$$Q_\tau(\omega) = \frac{2(a^2-\omega^2)}{(a^2+\omega^2)^2}.$$

Substituting these expressions in Equation (26) gives the ICI residual power as the oversampling factor, M, tends to infinity. The parameters used for the simulation are $\alpha = 0.7$, $a = 0.84$, $B\sigma_J = 0.1$, and $N = 512$. The generation of the correlated timing jitter sequence for simulation follows the idea developed in Appendix E. Figure 18 compares the performance of oversampling by factors of $M = 2, 100,$ and ∞. As we can see, oversampling reduces the ICI. However, when the timing jitter is correlated, this reduction comes to a limit, as indicated by the $M = \infty$ curve, beyond which the ICI cannot be reduced. Interestingly, oversampling by a factor of $M = 100$ instead of a factor of $M = 2$ only results in small further reduction in ICI power. This indicates that oversampling by a factor of $M = 2$ could be sufficient for most practical systems.

4.2 Adaptive Modulation

Despite the ability of oversampling to reduce ICI, it is obvious that practical systems can only oversample by less than a factor of four. This is because of the hardware restrictions on the possible sampling interval. Another way to deal with ICI is to exploit the non-uniform property of ICI power over subcarrier indexes for colored timing jitter.

The aim of adaptive modulation is to select the modulation order for a set of subcarriers based on the ICI power distribution. For instance, instead of using 16-QAM over all subcarriers, 4-QAM is used for a subset of the subcarriers where the ICI power is high, while 64-QAM is used for the remaining half, thereby maintaining the same data rate.

The improvement limitation of this scheme is based on the difference between the crest and trough on the ICI vs subcarrier index curve. The normalized distance of the 4-QAM, 16-QAM, and 64-QAM constellations are $\frac{2}{\sqrt{2}}$, $\frac{2}{\sqrt{10}}$, and $\frac{2}{\sqrt{42}}$ respectively. With this, the difference between the peak and low of the ICI curve has to be significant with respect to the ratio of the normalized distance between the 4-QAM and 64-QAM, which is approximately 13 dB, for the adaptive modulation scheme to yield substantial gain.

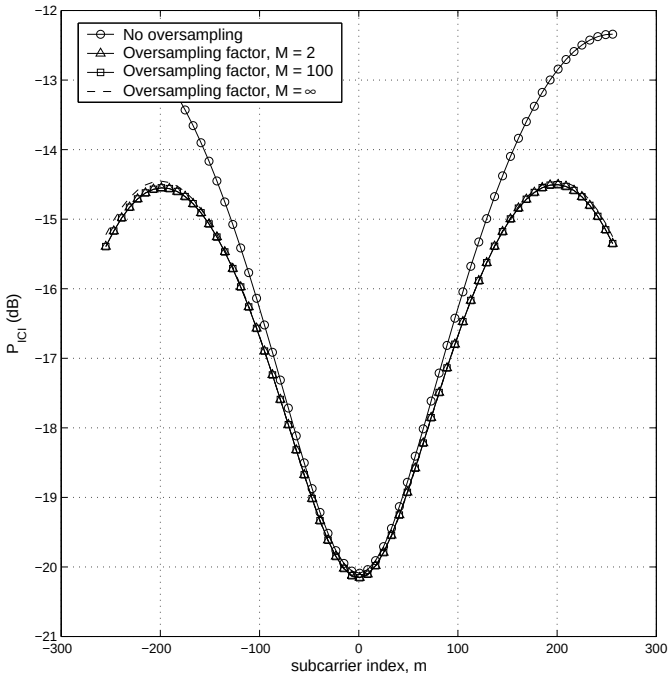

(a) Gaussian correlation

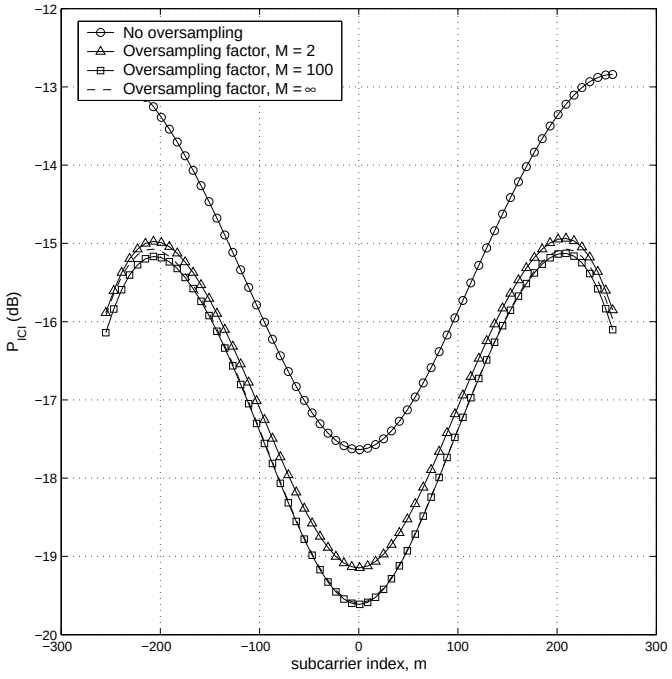

(b) exponential correlation

Figure 18. Variation of ICI power after oversampling versus subcarrier index

CHAPTER 5

REPERCUSSIONS OF PRACTICAL UWB ISSUES

In the previous chapters, we have analyzed and demonstrated the effects of timing jitter on UWB systems. These analysis were based on simplified channel models that makes the illustrations succinct and more mathematically tractable. However, when dealing with large-bandwidth systems, it is important to note that multipaths will be present. This in turn causes fading of the signals at the receiver. In this section, we present channel estimation and signal detection schemes designed to accommodate for the frequency-selective fading prevalent in UWB systems.

5.1 Channel Estimation

Here, we give a brief description of the prevalent practice used in signal detection involving channel estimation and interference suppression schemes. This sets the benchmark for the examples given in Section 5.4.

5.1.1 Channel Estimation in Impulse Radio

To detect UWB signal, parameters of UWB channel have to be estimated at receiver. Therefore, we will discuss channel estimation for single-carrier based modulation.

UWB channel response can be modelled by

$$h(t) = \sum_{l=1}^{L} \gamma_l \delta(t - \tau_l), \tag{27}$$

where γ_l and τ_l are the gain and the delay of the l-th path, respectively, L is the total number of resolvable propagation paths, and $\delta(.)$ is the Dirac delta function. When

a signal, $s(t)$, passes through a UWB channel, the channel output is

$$\begin{aligned} r(t) &= h(t) * s(t) + n(t) \\ &= \sum_{l=1}^{L} \gamma_l s(t - \tau_l) + n(t), \end{aligned} \tag{28}$$

where $n(t)$ is AWGN. To estimate channel parameters, training sequence will be used. In that case, transmitted signal, $s(t)$, is known to the receiver.

A number of channel estimation techniques have been proposed. We will describe two channel estimation approaches by Li, Molisch and Zhang in [22] and by Lottici, D'Andrea, and Mengali in [27], respectively.

Model based ML Channel Estimation

From (27), once amplitude gains, γ_l's, and delays, τ_l's, are known, the channel's impulse response can be determined. The algorithm in [27] makes maximum likelihood estimation to γ_l's and τ_l's.

During the training period, the transmitted signal, $s(t)$, is known to the receiver. By comparing it with the received signal, $r(t)$, a log-likelihood function is obtained, which is determined by

$$\begin{aligned} \log[\Lambda(\vec{\gamma}, \vec{\tau})] &= 2 \int_0^{KT_s} r(t) \left(\sum_{l=1}^{L} \tilde{\gamma}_l s(t - \tilde{\tau}_l) \right) dt \\ &\quad - \int_0^{KT_s} \left(\sum_{l=1}^{L} \tilde{\gamma}_l s(t - \tilde{\tau}_l) \right)^2 dt, \end{aligned} \tag{29}$$

where K is the number of training symbols, $\{\tilde{\gamma}_l\}_{l=1}^{L}$ and $\{\tilde{\tau}_l\}_{l=1}^{L}$ are realization of the gains and delays,

$$\vec{\gamma} = (\tilde{\gamma}_1, \tilde{\gamma}_2, ..., \tilde{\gamma}_L),$$

and

$$\vec{\tau} = (\tilde{\tau}_1, \tilde{\tau}_2, ..., \tilde{\tau}_L).$$

The values of the vectors, $\vec{\gamma}$ and $\vec{\tau}$, can be obtained by maximizing the log-likelihood function (29).

Note that the likelihood function is a complicated function of $\vec{\gamma}$ and $\vec{\tau}$, and there is no closed form or simple solution to the problem. Following is a practical approach to deal with the problem. First, for a given $\vec{\tau}$, find $\vec{\gamma}_o(\vec{\tau})$ that maximizes the likelihood function. And then by exhaustive searching find $\vec{\tau_o}$ that maximizes the log-likelihood function $\log[\Lambda(\vec{\gamma}_o(\vec{\tau}), \vec{\tau})]$. Once the optimum delay vectors, $\vec{\tau_o}$, is found, the optimum gain vector can be found by $\vec{\gamma}_o = \vec{\gamma}_o(\vec{\tau}_o)$. Details on this approach can be found in [27].

Low-Complexity Channel Estimation

The ML channel estimation introduced above has very good performance. However, it is too complicated to implement in UWB systems, which usually require low-complexity receivers. Here, we present a low-complexity approach developed in [22]. The receiver structure used for both the channel estimation and signal detection is shown in Fig. 19,

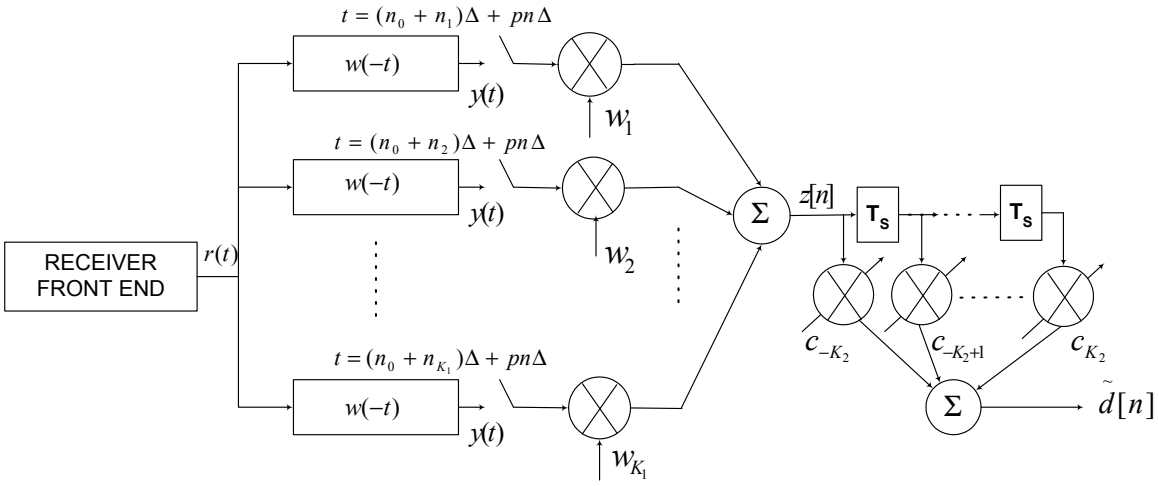

Figure 19. Receiver structure for channel estimation and signal detection.

For simplicity of discussion, amplitude modulation is assumed to be used. However, with only minor modification, the approach can be used in other types of modulation. Assume that $d_k \in \{+1, -1\}$ for $k = 0, \cdots, K-1$, are pseudo-random training

sequence. Then the transmitted signal

$$s(t) = \sum_{k=0}^{K-1} d_k w(t - kT_s),$$

where $w(t)$ is the spreading of the basic pulses. The expression of the received signal is similar to (28).

As shown in Fig. 19, to reduce the complexity at the receiver, an analog matched filter, matching $w(t)$, is used. Consequently, the output of the matched filter is

$$\begin{aligned} y(t) &= r(t) * w(-t) \\ &= \sum_{k=0}^{K-1} d_k \left(\sum_{l=1}^{L} \gamma_l \int_{-\infty}^{\infty} w(t - kT_s - \tau_l + \tau) w(\tau) d\tau \right) + \tilde{n}(t) \\ &= \sum_{k=0}^{K-1} d_k h(t - kT_s) + \tilde{n}(t) \end{aligned} \tag{30}$$

where

$$h(t) = \sum_{l=1}^{L} \gamma_l \int_{-\infty}^{\infty} w(t - \tau_l + \tau) w(\tau) d\tau,$$

and

$$\tilde{n}(t) = n(t) * w(-t).$$

The baud-rate sampled version of the analog matched filter output at each finger can be observed and used in channel estimation and signal detection, which can be expressed as

$$y(t_i + nT_s) = \sum_{k=0}^{K-1} d_k h(t_i + nT_s - kT_s) + \tilde{n}(t_i + nT_s),$$

where t_i is the timing of the finger. However, much denser than baud-rate sampled version of UWB channel is required for signal detection. Therefore, we have to estimate $h(l\Delta)$, where $\Delta = \frac{T_s}{p}$ for some integer p.

To estimate, $h(l\Delta)$, we need to obtain a denser sampled version of the matched filter $y(l\Delta)$ first. To get denser sampling, we use the channel sounding method proposed in [10, 22], which repeatedly sends the same training sequence and adjusts the

timing of each finger, t_i, to obtain $y(l\Delta)$. Once $y(l\Delta)$ is obtained, channel parameter can be estimated by

$$\tilde{h}(l\Delta) = \frac{1}{K}\sum_{k=0}^{K-1} d_k y(l\Delta + kT_s).$$

For pseudo-random training sequence, d_k, we have

$$\frac{1}{K}\sum_{k=0}^{K-1} d_k d_{k-k'} \approx \delta[k'],$$

then

$$\begin{aligned}
\tilde{h}(l\Delta) &= \frac{1}{K}\sum_{k=0}^{K-1} d_k \left(\sum_{m=0}^{K-1} d_m h(l\Delta + kT_s - mT_s) + \tilde{n}(l\Delta + kT_s)\right) \\
&= \frac{1}{K}\sum_{k=0}^{K-1}\sum_{m=0}^{K-1} d_k d_m h(l\Delta + (k-m)T_s) + \frac{1}{K}\sum_{k=0}^{K-1} d_k \tilde{n}(l\Delta + kT_s) \\
&= \sum_{k'} \underbrace{\frac{1}{K}\sum_{k=0}^{K-1} d_k d_{k-k'}}_{\approx\delta[k']} h(l\Delta + k'T_s) + \hat{n}(l\Delta) \\
&\approx h(l\Delta) + \hat{n}(l\Delta), \qquad (31)
\end{aligned}$$

where

$$\hat{n}(l\Delta) = \frac{1}{K}\sum_{k=0}^{K-1} d_k \tilde{n}(l\Delta + kT_s),$$

is the effect of channel noise.

Fig. 20, from [22], shows the performance of the low-complexity channel estimator. In the simulated system, the 5th derivative of the Gaussian function with $\sigma = 5.28 \times 10^{-11}$ sec is used. The chip duration is $T_c = 0.625$ nsec. The length of spreading sequence is $N = 8$; therefore, the symbol during is $T_s = 8T_c = 5$ nsec. The impulse response of UWB channel is over-sampled 32 times ($p = 32$). The analog rake receiver has $K_1 = 10$ fingers. The training sequence, consisting 511 symbols, is repeated 4 times to obtain 32 time over-samples. The work shows that the effect of channel estimation error using this technique will be negligible for signal detection.

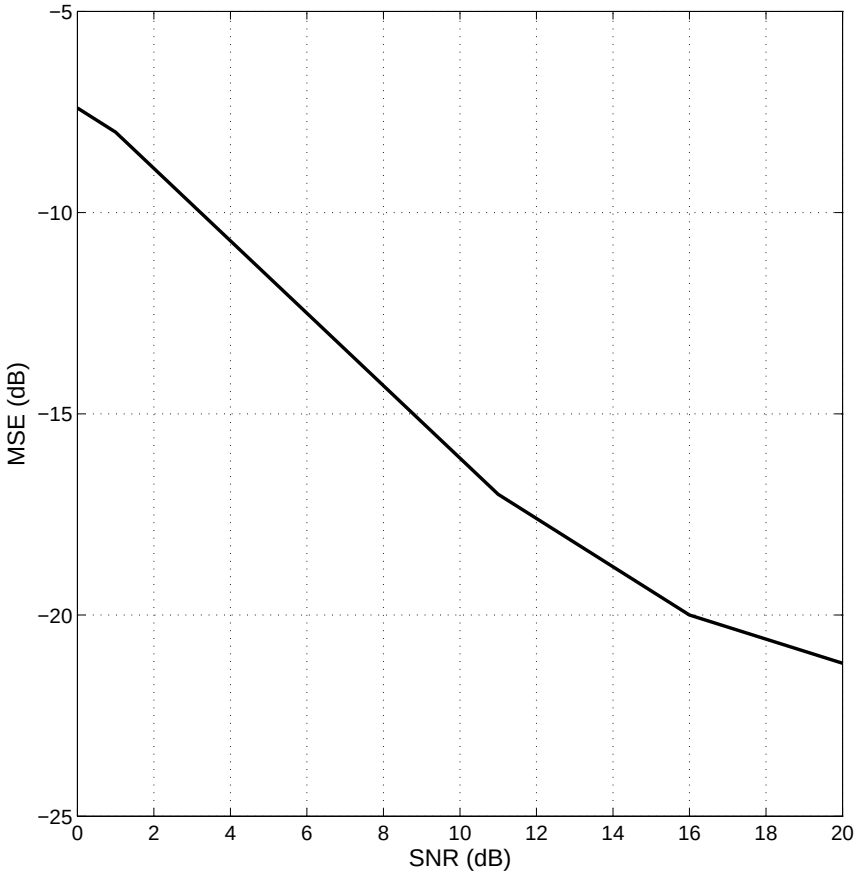

Figure 20. Performance of the low-complexity channel estimation technique in [22].

5.1.2 Channel Estimation in OFDM-based UWB

Channel estimation for OFDM based wireless communications has been investigated in [20] and the references therein. However, for OFDM based UWB communications, low-complexity channel estimate is desired. Here, we present the estimator developed in [23].

In UWB communications, channel can be regarded stationary or quasi-stationary. Therefore, channel tracking is not necessary. Channel estimation is performed during the training period. During the training period, the transmitted symbols are known to the receiver, which can be used to get a temporal estimation of channel parameters by

$$\tilde{H}_k = \frac{r_k}{d_k} = H_k + \tilde{n}_k,$$

where

$$\tilde{n}_k = \frac{n_k}{d_k}.$$

Then, taking an *inverse DFT* (I-DFT), we have: $\{\tilde{h}_n\}_{n=0}^{N-1} = \text{I-DFT}\{\tilde{H}_k\}_{k=0}^{N-1}$.

Let the delay profile of UWB channel be p_n, which is determined by environment and can be estimated in practical situation. With the delay profile, it is possible to further reduce the noise level by defining a new estimate

$$\hat{h}_n = \frac{p_n}{p_n + \Delta}\tilde{h}_n,$$

where Δ is noise (including interference) power and can be estimated by

$$\Delta = \frac{1}{N_2 - N_1 - 1}\sum_{n=N_1}^{N_2}\left|\tilde{h}_n\right|^2.$$

Figure 21 shows the MSE of the above channel estimator. The parameters of the OFDM based UWB are described in [23].

5.2 Signal Detection

Fig. 19 shows a signal detector with K_1 fingers for rake receiver and $2K_2+1$ taps for equalizer for a UWB system with amplitude modulation (AM), which is a combination of rake receiver and channel equalizer.

Let $h(n_k\Delta)$, for $k = 1, \cdots, K_1$, be the K_1 taps with the largest $|\hat{h}(n_k\Delta)|$. If the weighs for the rake fingers are $\{w_k\}_{k=1}^{K_1}$, then the rake output can be expressed as

$$z[n, n_o] = \sum_{k=1}^{K_1} w_k y((n_o + n_k)\Delta + nT_s),$$

where $n_o\Delta$ is the timing of the whole RAKE receiver.

For traditional *maximal ratio* (MR) rake receiver, $n_o = 0$ and $w_k = h^*(n_k\Delta)$. To improve its performance, *minimum mean-square-error* (MMSE) rake combining can be used. In that case, the weights and timing are determined by minimizing

$$MSE(\mathbf{w}, n_o) \quad = \quad \frac{1}{K}\sum_{k=0}^{K-1}\left|z[k, n_o] - d_k\right|^2, \tag{32}$$

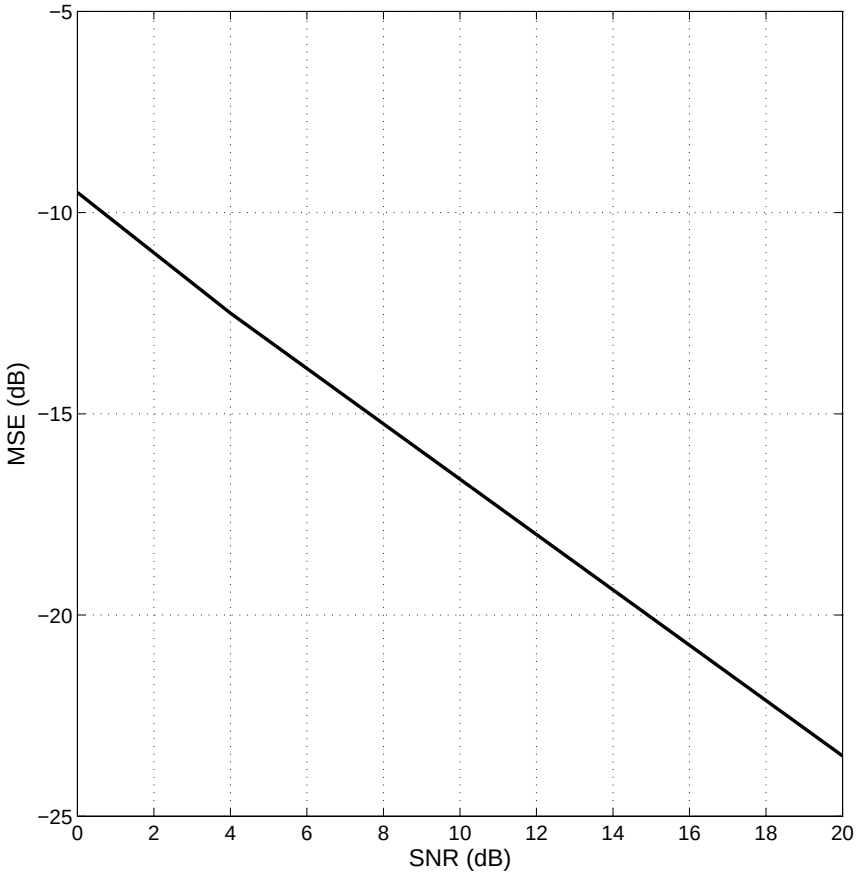

Figure 21. Channel estimation performance for an OFDM based UWB system.

where $\mathbf{w} = (w_1, \cdots, w_{K_1})$ is the rake weights vector. Therefore, for a fixed timing, n_o, the optimum weight vector can be determined by

$$\mathbf{w}_o[n_o] = \left(\mathbf{Y}[n_o]\mathbf{Y}^H[n_o]\right)^{-1}\left(\mathbf{Y}[n_o]\mathbf{d}^H\right),$$

where $\mathbf{d} = (d_0, \cdots, d_{K-1})$ is the training vector and

$$\mathbf{Y}[n_o] = \begin{pmatrix} y((n_1+n_o)\Delta) & \dots & y((K-1)T_s + (n_1+n_o)\Delta) \\ y((n_2+n_o)\Delta) & \dots & y((K-1)T_s + (n_2+n_o)\Delta) \\ \vdots & \dots & \vdots \\ y((n_{K_1}+n_o)\Delta) & \dots & y((K-1)T_s + (n_{K_1}+n_o)\Delta) \end{pmatrix}.$$

Then optimum timing is found by minimizing $MSE(\mathbf{w}_o[n_o], n_o)$.

To further mitigate residual intersymbol interference of the rake receiver output, a short *minimum MSE* (MMSE) equalizer is used after it. The coefficients of the

MMSE equalizer are found by minimizing

$$MSE(\mathbf{c}, n_o) = \frac{1}{K} \sum_{n=0}^{K-1} \left| \sum_{k=-K_2}^{K_2} c_k z[n-k, n_o] - d_n \right|^2,$$

where $\mathbf{c} = (c_{-K_2}, \cdots, c_0, \cdots, c_{K_2})$ is the equalizer coefficient vector. Therefore,

$$\mathbf{c} = \left(\sum_{k=0}^{K-1} \mathbf{z}_k {\mathbf{z}_k}^T \right)^{-1} \left(\sum_{k=0}^{K-1} \mathbf{z}_k d_k \right). \tag{33}$$

where the output vector

$$\mathbf{z}_n = \begin{pmatrix} z[n+K_2, n_o] \\ \vdots \\ z[n-K_2, n_o] \end{pmatrix}.$$

More details on this signal detector can be found in [22]. Fig. 22 compares the BER performance of MMSE and MR rake combining for CM-3 and CM-4 channel models [1], respectively. The UWB system is the same as the one for channel estimation (at the end of Section 2.2.3). Rake receiver for signal detector uses $K_1 = 10$ fingers implemented by analog device, and the equalizer has five taps ($K_2 = 2$). From the figure, we can see that the MMSE rake receiver has much better performance than the MR rake receiver. In particular, the required SNR for a 1% BER has about 6 dB improvement for the CM-4 channel model.

5.3 Interference Suppression for OFDM-based UWB

For an OFDM-based UWB system with sub-band repetition diversity [23] or receive antenna arrays, the system also has ability to suppress interference besides diversity gain. In this case, the received signal at the k-th subcarrier can be expressed as

$$r_k^{(l)} = H_k^{(l)} d_k + n_k^{(l)}, \tag{34}$$

for $l = 1, \cdots, L$, where l is the antenna or sub-band index, $n_k^{(l)}$ includes AWGN and co-channel or multi-user interference, which is therefore not *spatially* white any more.

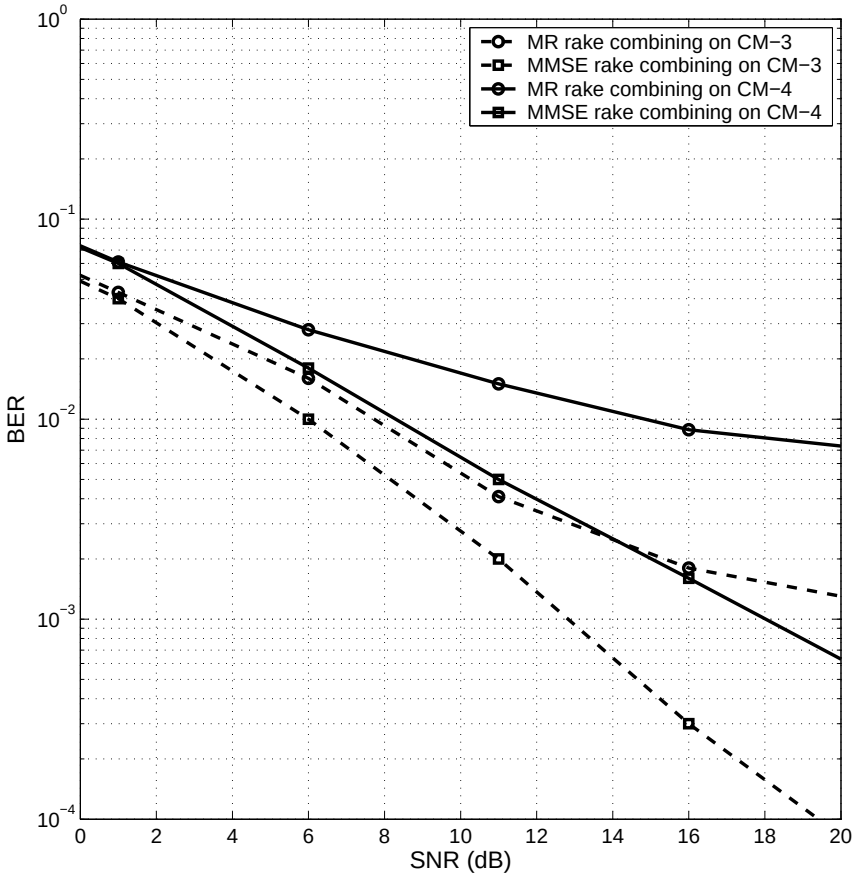

Figure 22. Comparison of MMSE and MR signal detection techniques.

The spatial correlation of $n_k^{(l)}$ can be used to improve system performance by finding combining weights, $w_k^{(l)}$'s, to minimize

$$\text{MSE}(\mathbf{w}_k) = E\left|\mathbf{w}_k^H \mathbf{r}_k - d_k\right|^2, \tag{35}$$

where

$$\mathbf{r}_k = \begin{pmatrix} r_k^{(1)} \\ \vdots \\ r_k^{(L)} \end{pmatrix} \quad \text{and} \quad \mathbf{w}_k = \begin{pmatrix} w_k^{(1)} \\ \vdots \\ w_k^{(L)} \end{pmatrix}.$$

In reality, time average is used instead of assemble average in (35) to find combining weights. Approaches for single-carrier [43] and for OFDM [24] have been developed. However, as indicated in [23], those approaches can not be directly used in OFDM based UWB systems. Therefore, we introduce the approach in [23] here.

To exploit the correlation of UWB channel frequency responses at different sub-channels, we estimate combining weights to minimize the following cost function

$$\mathcal{C}(\mathbf{w}_k) = \frac{1}{\sum_n \lambda^{|n-k|}} \sum_n \lambda^{|n-k|} \left| \mathbf{w}_k^H \mathbf{r}_n - d_n \right|^2, \tag{36}$$

where λ is a forgetting factor between 0 and 1, depending on channel's frequency selectivity. It is smaller for channel with larger frequency selectivity. Direct calculation to (36) yields that

$$\mathbf{w}_k = \mathbf{R}_k^{-1} \mathbf{a}_k,$$

where the correlation matrix and vector are defined respectively as,

$$\mathbf{R}_k = \frac{1}{\sum_n \lambda^{|n-k|}} \sum_n \lambda^{|n-k|} \mathbf{r}_n \mathbf{r}_n^H$$

and

$$\mathbf{a}_k = \frac{1}{\sum_n \lambda^{|n-k|}} \sum_n \lambda^{|n-k|} \mathbf{r}_n s_n^*.$$

Once the combining coefficients are found, received signals from difference antennas or sub-bands can be combined by

$$x_k = \mathbf{w}_k^H \mathbf{r}_k.$$

It is important to note that besides the above OFDM based UWB modulation, another modified version of OFDM has been also proposed for multiple access of UWB systems in [6, 35]. With these brief description of practical issues considered by communication engineers, we hightlight the features using simulations in the next section (Section 5.4).

5.4 Practical Examples

As has been mentioned in this chapter, the analysis that has been carried out in previous chapters were based on simplified mathematical models - one that ignores frequency-selectivity of the channel. In true UWB systems, multipath is an unavoidable fact and has to be accounted for by the communication engineers. Even with

OFDM-based UWB systems, the fading experienced by a subcarrier in a sub-band is still frequency selective. Consider the fact that FCC definitions limits the minimum bandwidth for each sub-band of OFDM-based UWB to 512 MHz. This means that by even using 512 subcarriers/tones per sub-band, the allocated minimum band of 1 MHz is large enough to necessitate a frequency-selective model unless a long enough cyclic prefix is assigned to the OFDM symbols. In this section, we present two different examples of a practical OFDM-based UWB taking frequency selectivity into account where no cyclic prefix is attached.

5.4.1 CASE 1: N = 32, Delay Spread = 10 ns

There are a number literature works on the channel models for UWB channels [40], [9]. One common ground of agreement in most UWB channel models is that the amplitude of the multipath gains are no longer considered mere Rayleigh or Ricean fading. Instead Nakagami-m or log-normal fading coefficients are assumed. This is due to the fact that the time resolution of UWB is much finer than its narrowband counterpart. Therefore, the assumption that the number of paths arriving within a time-bin is large enough for the Central Limit Theorem assumption to be made on the complex multipath gains is not exactly valid.

In this case study, we performed simulation with the number of subcarriers, N = 32. The basic symbols were selected from a binary phase-shift-keying (BPSK) scheme. The channel is frequency selective with the delay spread being 10 ns. The power delay profile is an exponential decay with each multipath gain taking a log-normal random variable. In essense, the received signal is modified from Equation (11)

$$\hat{s}_m = \frac{1}{N} \sum_{n=-\frac{N}{2}+1}^{\frac{N}{2}} \left(\sum_{l=1}^{L} \beta_l s(t-\varepsilon_l) + w(t) \Big|_{t=n\Delta t+\tau_n} \right) \exp\left(-j\frac{2\pi mn}{N}\right),$$

where $w(t)$ is the additive channel noise, ε_l is the time delay due to the l-th multipath, β_l is the log-normal gain associated with it, and L is the total number of paths in the receive window. In this case study, $\varepsilon_L = 10\ ns$. The simulation result is

shown in Fig. 23. In this simulation, equalization was done at the receiver with a

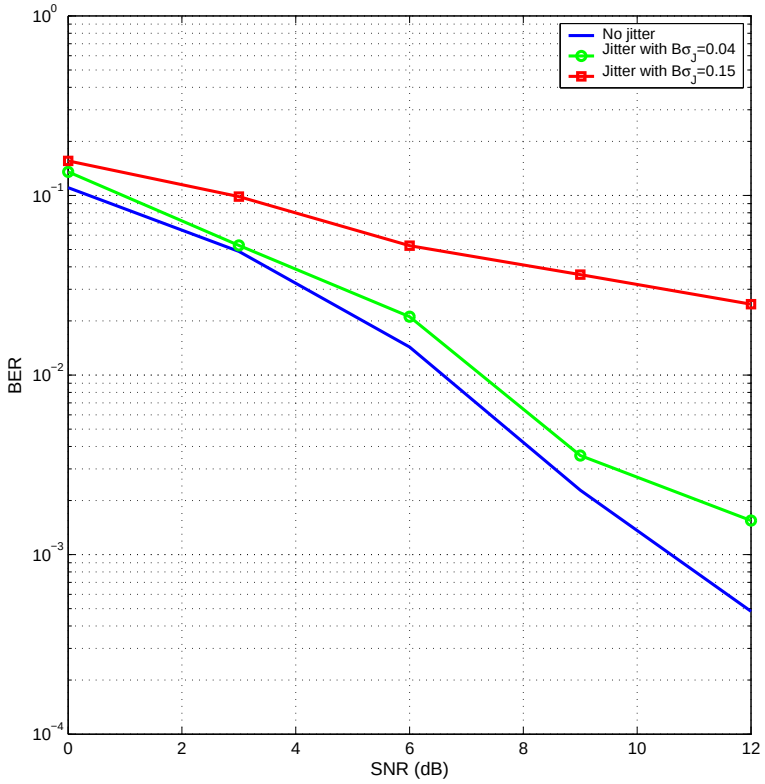

Figure 23. BER performance under Frequency Selective channel using Equalizer in Fig 19; Number of subcarriers, N = 32, delay spread = 10 ns

training sequence of length 200 used to obtain the coefficients of the FIR equalizer. Figure 23 shows that the damaging effect of timing jitter could be very substantial unless measures, such as oversampling and/or adaptive modulation proposed in our work, are taken to mitigate it.

5.4.2 CASE 2: N = 16, Delay Spread = 50 ns

The simulation setup is essentially the same with Section 5.4.1, except that the delay spread is more over a longer time frame of 50 ns. Also, the number of subcarriers have been reduced to 16 and the training sequence is of length 500 to cater for the longer delay spread. The results are shown in Fig. 24. Once again, the underlying fault of these systems are the $B\sigma_J$ product influenced by the timing jitter RMS, σ_J. It is worthy to note that these practical examples do not provide an exhaustive field of

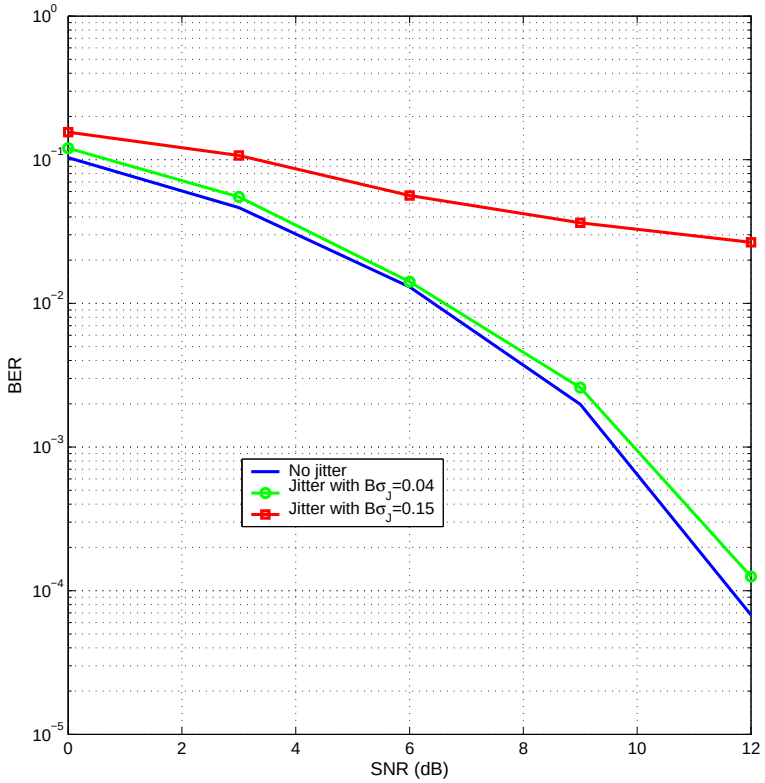

Figure 24. BER performance under Frequency Selective channel; Number of subcarriers, N = 16, delay spread = 50 ns

considerations by communication engineers. Other factors worth taking into account are the effects and mitigation of narrowband interference [33] and the limitations of oversampling achievable at the analog-to-digital converter (ADC) [39].

CHAPTER 6

CONCLUSION

This concluding chapter summarizes the main contributions of this thesis work. We have, through this work, shown that the effect of timing jitter can be very significant for UWB systems and hence form an important consideration for real-time UWB communication systems. The specific contribution of this thesis are listed below

- Optimum modulation index for impulse radio PPM
- Timing jitter effect on impulse radio
- Timing jitter effect on OFDM-based UWB
- Techniques for mitigating performance loss in UWB due to timing jitter

In Chapter 2, we showed that timing jitter can cause great system degradation for impulse radio. In the case of pulse-position modulation (PPM), timing jitter destroys the correlation property substantially with respect to the modulation index. This proved to be more pronounced for the highly time-sensitive fourth-order Gaussian pulse. It also indicates that the quantity of the minimum correlation of the transmitted basis signal is not enough for judging the performance but rather the timing sensitivity of the correlation function is a new dimension that has to be considered also. Chapter 2 then showed how the performance degradation can be mitigated using a combination of pulse-shaping and sample averaging techniques. These techniques provide little overhead but yield great dividends in SNR gain.

In Chapter 3, we extend the study of timing jitter to OFDM-based UWB systems. This introduced a phenomenon known as interchannel interference (ICI), which degrades the system performance by cross-linking symbols from different subcarriers as

interference. We developed a novel approach to the problem and obtained a universal bound on this ICI. It was shown that the major terms playing a key role in the ICI power are the bandwidth allocated to the sub-bands and the RMS of the timing jitter. We then proposed in Chapter 4 two techniques for reducing the effect of this timing jitter-induced ICI - oversampling and adaptive modulation. The simplicity of the techniques of oversampling and adaptive symbol modulation makes it a readily available solution for reducing ICI induced by timing jitter.

In the detailed analysis of this work, simplified channel models were used to keep the results mathematically tractable. However, to merge with real world issues, Chapter 5 was added to give insights on practical aspects important to the communication engineers. This chapter then concludes by providing examples that justify the effects of timing jitter considered in prior chapters.

APPENDIX A

DERIVATION OF EQUATION (3)

We have $p(t) = A\frac{t}{\sigma^2}e^{-\frac{t^2}{2\sigma^2}}$, so that

$$\begin{aligned} R_1(\delta) &\approx \frac{1}{E_p}\int_{-\infty}^{\infty} p(t)p(t-\delta)dt \\ &= \frac{A^2}{\sigma E_p}\int_{-\infty}^{\infty} te^{-\frac{t^2}{2}}\cdot(t-\delta)e^{-\frac{(t-\delta)^2}{2}}dt \\ \Rightarrow \frac{\sigma E_p}{A^2}R_1(\delta) &= \int_{-\infty}^{\infty}(t^2-\delta t)e^{-frac12[2t^2+\delta^2-2t\delta]}dt \\ &= e^{-\frac{\delta^2}{2}}\int_{-\infty}^{\infty} t^2e^{-t^2+\delta t}dt - \delta e^{-\frac{\delta^2}{2}}\int_{-\infty}^{\infty} te^{-t^2+\delta t}dt, \end{aligned}$$

which from (3.462-2) and (3.462-6) (pg. 360, 361) in [14] can be simplified to

$$\begin{aligned} \frac{\sigma E_p}{A^2}R_1(\delta) &= e^{-\frac{\delta^2}{2}}\left(2!e^{\frac{\delta^2}{4}}\sqrt{\pi}\left(\frac{\delta}{2}\right)^2\sum_{k=0}^{1}\frac{1}{(2-2k)!k!}\left(\frac{1}{\delta^2}\right)^k\right) - \delta e^{-\frac{\delta^2}{2}}\left(\frac{\delta}{2}\sqrt{\pi}e^{\frac{\delta^2}{4}}\right) \\ \Leftrightarrow R_1(\delta) &= \frac{A^2\sqrt{\pi}}{\sigma E_p}(0.5-\pi^2\alpha^2)\exp(-\pi^2\alpha^2), \end{aligned}$$

where the substitution $\delta = 2\pi\alpha$ was done in the final equation.

APPENDIX B

DERIVATION OF ICI POWER FOR COLORED TIMING JITTER

Substituting $f_k = k\frac{B}{N}$ into (21), we have

$$\begin{aligned} P_{ICI}(m) &= \frac{\sigma_s^2}{N^2}\sum_{k\neq m}\left\{N + 2\sum_{l=1}^{N-1} l\left[1 - 4\pi^2(B\sigma_J)^2\left(\frac{k}{N}\right)^2(1-\rho_{N-l})\right]\cos\frac{2\pi}{N}(k-m)l\right\} \\ &= \frac{\sigma_s^2}{N^2}\sum_{k\neq m}\left\{N + 2\sum_{l=1}^{N-1} l\left[1 - 4\pi^2(B\sigma_J)^2\left(\frac{k}{N}\right)^2(1-\rho_{N-l})\right]\right. \\ &\quad \left.\times\left[2\cos^2\left(\frac{\pi}{N}(k-m)l\right) - 1\right]\right\} \\ &= \frac{\sigma_s^2}{N^2}\sum_{k\neq m} N + 4\sum_{l=1}^{N-1} l\left[1 - 4\pi^2(B\sigma_J)^2\left(\frac{k}{N}\right)^2(1-\rho_{N-l})\right]\cos^2\left(\frac{\pi(k-m)l}{N}\right) \\ &\quad -2\sum_{l=1}^{N-1} l\left[1 - 4\pi^2(B\sigma_J)^2\left(\frac{k}{N}\right)^2(1-\rho_{N-l})\right] \qquad (37) \\ &= \frac{\sigma_s^2}{N^2}\sum_{k=-\frac{N}{2}+1,k\neq m}^{\frac{N}{2}}(N + 4\Lambda(k) - 2\Gamma(k)), \qquad (38) \end{aligned}$$

where

$$\Lambda(k) = \sum_{l=1}^{N-1} l\left[1 - 4\pi^2(B\sigma_J)^2\left(\frac{k}{N}\right)^2(1-\rho_{N-l})\right]\cos^2\left(\frac{\pi}{N}(k-m)l\right)$$

and

$$\Gamma(k) = \sum_{l=1}^{N-1} l\left[1 - 4\pi^2(B\sigma_J)^2\left(\frac{k}{N}\right)^2(1-\rho_{N-l})\right].$$

$\Lambda(k)$ and $\Gamma(k)$ can be simplified by the following

$$\begin{aligned}
\Lambda(k) &= \sum_{l=1}^{N-1} l\left[1-4\pi^2(B\sigma_J)^2\left(\frac{k}{N}\right)^2(1-\rho_{N-l})\right]cos^2\left(\frac{\pi}{N}(k-m)l\right) \\
&= \underbrace{\sum_{l=1}^{N-1} l\cdot cos^2\left(\frac{\pi}{N}(k-m)l\right)}_{\frac{N}{2}\left(\frac{N}{2}-1\right)\text{ since } m\neq k} \\
&\quad -4\pi^2(B\sigma_J)^2\left(\frac{k}{N}\right)^2\sum_{l=1}^{N-1} l\,(1-\rho_{N-l})\,cos^2\left(\frac{\pi}{N}(k-m)l\right) \\
&= \frac{N}{2}\left(\frac{N}{2}-1\right)\left[1-4\pi^2(B\sigma_J)^2\left(\frac{k}{N}\right)^2\right] \\
&\quad +4\pi^2(B\sigma_J)^2\left(\frac{k}{N}\right)^2\sum_{l=1}^{N-1} l\rho_{N-l}cos^2\left(\frac{\pi}{N}(k-m)l\right),
\end{aligned}$$

and

$$\begin{aligned}
\Gamma(k) &= \sum_{l=1}^{N-1} l\left[1-4\pi^2(B\sigma_J)^2\left(\frac{k}{N}\right)^2(1-\rho_{N-l})\right] \\
&= \sum_{l=1}^{N-1} l-4\pi^2(B\sigma_J)^2\left(\frac{k}{N}\right)^2\sum_{l=1}^{N-1} l(1-\rho_{N-l}) \\
&= \frac{N(N-1)}{2}-4\pi^2(B\sigma_J)^2\left(\frac{k}{N}\right)^2\left[\frac{N(N-1)}{2}-\sum_{l=1}^{N-1} l\rho_{N-l}\right] \\
&= \frac{N(N-1)}{2}\left[1-4\pi^2(B\sigma_J)^2\left(\frac{k}{N}\right)^2\right]+4\pi^2(B\sigma_J)^2\left(\frac{k}{N}\right)^2\sum_{l=1}^{N-1} l\rho_{N-l}.
\end{aligned}$$

Substituting the simplified expressions of $\Lambda(k)$ and $\Gamma(k)$ into (38), the general expression for the ICI power caused by colored timing jitter is

$$P_{ICI}(m)=\frac{\sigma_s^2}{N}\sum_{k\neq m}\left\{4\pi^2(B\sigma_J)^2\left(\frac{k}{N}\right)^2\left[1+\frac{2}{N}\sum_{l=1}^{N-1} l\cdot\cos\left(2\pi\frac{l}{N}(k-m)\right)\rho_{N-l}\right]\right\}.$$

Furthermore,

$$P_{ICI}(m) = 4\pi^2(B\sigma_J)^2\sigma_s^2\frac{1}{N}\sum_{k=-\frac{N}{2}+1,k\neq m}^{\frac{N}{2}}\left(\frac{k}{N}\right)^2 + \frac{\sigma_s^2}{N}\left(\frac{2}{N}\right)4\pi^2(B\sigma_J)^2\sum_{l=1}^{N-1}l\rho_{N-l}\sum_{k=-\frac{N}{2}+1,k\neq m}^{\frac{N}{2}}\left(\frac{k}{N}\right)^2\cos\left(2\pi\frac{l}{N}(k-m)\right)$$

$$= 4\pi^2(B\sigma_J)^2\sigma_s^2\cdot\frac{1}{12}\left[1+\frac{1}{N^2}-\frac{12}{N}\left(\frac{m}{N}\right)^2\right] + \frac{\sigma_s^2}{N}\left(\frac{2}{N}\right)4\pi^2(B\sigma_J)^2\sum_{l=1}^{N-1}l\rho_{N-l}\left[\frac{\cos\left(\frac{2\pi l}{N}m\right)}{N^2}\cdot\frac{(-1)^lN}{2\sin^2\left(\frac{\pi l}{N}\right)}-\left(\frac{m}{N}\right)^2\right]. \quad (39)$$

Neglecting the $\left(\frac{m}{N}\right)^2$ and $\frac{2}{N^2}$ terms, since they become insignificant for large N compared to the terms they are added to, we have the simplification

$$\frac{P_{ICI}(m)}{\sigma_s^2} = \frac{\pi^2}{3}(B\sigma_J)^2\left[1+\frac{12}{N^3}\sum_{l=1}^{N-1}(-1)^l l\rho_{N-l}\frac{\cos\left(\pi\frac{l}{N}2m\right)}{\sin^2\left(\pi\frac{l}{N}\right)}\right].$$

APPENDIX C

DERIVATION OF EQUATION (23)

Recall that from Equation 39 in Appendix B that

$$\begin{aligned}\frac{P_{ICI}(m)}{\sigma_s^2} &= 4\pi^2(B\sigma_J)^2 \cdot \frac{1}{12}\left[1+\frac{1}{N^2}-\frac{12}{N}\left(\frac{m}{N}\right)^2\right] \\ &\quad + \frac{1}{N}\left(\frac{2}{N}\right)4\pi^2(B\sigma_J)^2\sum_{l=1}^{N-1} l\rho_{N-l}\left[\frac{\cos\left(\frac{2\pi l}{N}m\right)}{N^2}\cdot\frac{(-1)^l N}{2\sin^2\left(\frac{\pi l}{N}\right)}-\left(\frac{m}{N}\right)^2\right].\end{aligned}$$

$$\begin{aligned}&= \frac{\pi^2}{3}(B\sigma_J)^2\left[1+\frac{1}{N^2}-\frac{12}{N}\left(\frac{m}{N}\right)^2\right]+ \\ &\quad \frac{8\pi^2(B\sigma_J)^2}{N^3}\left\{\sum_{l=1}^{N-1}(-1)^l l\rho_{N-l}\frac{\cos\left(\pi\frac{l}{N}2m\right)}{2\sin^2\left(\pi\frac{l}{N}\right)}-\frac{m^2}{N}\sum_{l=1}^{N-1} l\rho_{N-l}\right\}.\end{aligned}$$

When the number of subcarriers is not assumed very large, a better approximation to make is set

$$\frac{P_{ICI}(m)}{\sigma_s^2} \approx \frac{\pi^2}{3}(B\sigma_J)^2+\frac{8\pi^2(B\sigma_J)^2}{N^3}\left\{\sum_{l=1}^{N-1}(-1)^l l\rho_{N-l}\frac{\cos\left(\pi\frac{l}{N}2m\right)}{2\sin^2\left(\pi\frac{l}{N}\right)}-\frac{m^2}{N}\sum_{l=1}^{N-1} l\rho_{N-l}\right\}$$

Averaging this over the subcarriers m then gives

$$\begin{aligned}\frac{\bar{P}_{ICI}}{\sigma_s^2} &\approx \frac{\pi^2}{3}(B\sigma_J)^2-\frac{8\pi^2(B\sigma_J)^2}{N^2}\sum_{l=1}^{N-1} l\rho_{N-l}\frac{1+\frac{1}{N^2}}{12} \\ &= \frac{\pi^2(B\sigma_J)^2}{3}\left[1-\frac{2}{N^2}\sum_{l=1}^{N-1} l\rho_{N-l}\left(1+\frac{1}{N^2}\right)\right] \qquad (40)\end{aligned}$$

Equation (40) indicates that the average ICI power actually experienced for colored timing jitter can be less than its uncorrelated counterpart. However, this is based on the sign of the summation $\sum_{l=1}^{N-1} l\rho_{N-l}$. For the correlation functions used in this work, this sum will always be positive and hence simulation results based on $N \leq 32$ will show significant difference between the average ICI power for colored timing jitter and the white timing jitter line.

APPENDIX D

PROOF THAT COLORED NOISE HAS NO EFFECT ON ICI FOR OFDM-BASED UWB

Without noise, the demodulated OFDM signal is given as

$$\begin{aligned}\hat{s}_m &= \frac{1}{N}\sum_{n=-\frac{N}{2}}^{\frac{N}{2}} s\left(n\Delta t+\tau_n\right)e^{-j\frac{2\pi mn}{N}} \\ &= \sum_{k=-\frac{N}{2}+1}^{\frac{N}{2}} s_k\left(\frac{1}{N}\sum_{n=-\frac{N}{2}+1}^{\frac{N}{2}} e^{j\frac{2\pi}{N}(k-m)n}\cdot e^{j2\pi f_k\tau_n}\right),\end{aligned}$$

where the substitution $s(n\Delta t+\tau_n)=\sum_{k=-\frac{N}{2}+1}^{\frac{N}{2}} s_k e^{j\left(\frac{2\pi kn}{N}+2\pi f_k\tau_n\right)}$ has been made.

If we have noise, then the demodulated signal becomes

$$\begin{aligned}\hat{s}_m &= \frac{1}{N}\sum_{n=-\frac{N}{2}}^{\frac{N}{2}}\left[\sum_{k=-\frac{N}{2}+1}^{\frac{N}{2}} s_k e^{j\left(\frac{2\pi kn}{N}+2\pi f_k\tau_n\right)}+w(n\Delta t+\tau_n)\right] \\ &= \sum_{k=-\frac{N}{2}+1}^{\frac{N}{2}} s_k\left(\frac{1}{N}\sum_{n=-\frac{N}{2}}^{\frac{N}{2}} e^{j\frac{2\pi(k-m)n}{N}}\cdot e^{j2\pi f_k\tau_n}\right) \\ &\quad +\frac{1}{N}\sum_{n=-\frac{N}{2}}^{\frac{N}{2}}\underbrace{w(n\Delta t+\tau_n)}_{\text{noise term}}e^{-j\frac{2\pi mn}{N}} \\ &= \underbrace{s_m\left(\frac{1}{N}\sum_{n=-\frac{N}{2}}^{\frac{N}{2}} e^{j2\pi f_k\tau_n}\right)}_{\eta}+\underbrace{\sum_{\substack{k=-\frac{N}{2}+1\\ k\neq m}}^{\frac{N}{2}} s_k\left(\frac{1}{N}\sum_{n=-\frac{N}{2}}^{\frac{N}{2}} e^{j\frac{2\pi(k-m)n}{N}}\cdot e^{j2\pi f_k\tau_n}\right)}_{\alpha_m} \\ &\quad +\underbrace{\frac{1}{N}\sum_{n=-\frac{N}{2}}^{\frac{N}{2}} w(n\Delta t+\tau_n)e^{-j\frac{2\pi mn}{N}}}_{w_m}.\end{aligned}$$

The mean-square value of the demodulated signal is then

$$\begin{aligned}\mathbf{E}\left\{|\hat{s}_m|^2\right\} &= \mathbf{E}\left\{|\eta s_m + \alpha_m + w_m|^2\right\} \\ &= \mathbf{E}\left\{|\eta s_m|^2 + w_m^* \eta s_m + |\alpha_m|^2 + \alpha_m w_m^* + |w_m|^2\right\}\end{aligned}$$

since $\mathbf{E}\{\alpha_m^* \eta s_m\} = \mathbf{E}\{\alpha_m \eta^* s_m^*\} = 0$. Splitting the expectation equation above, we have

$$\begin{aligned}\mathbf{E}\left\{|\hat{s}_m|^2\right\} = & \underbrace{\mathbf{E}\left\{|\eta s_m|^2\right\} + \mathbf{E}\{w_m^* \eta s_m\}}_{\text{contributes to desired signal energy}} + \underbrace{\mathbf{E}\left\{|\alpha_m|^2\right\} + \mathbf{E}\{\alpha_m w_m^*\}}_{\text{contributes to ICI}} \\ & + \underbrace{\mathbf{E}\left\{|w_m|^2\right\}}_{\text{noise strength}}\end{aligned}$$

Our main focus is on the part contributing to ICI given by

$$P_{ICI} = \mathbf{E}\left\{|\alpha_m|^2\right\} + \mathbf{E}\{\alpha_m w_m^*\}.$$

The first part of the equation is identical to the case without noise. For the second part of ICI,

$$\begin{aligned}\mathbf{E}\{\alpha_m w_m^*\} &= \frac{1}{N^2}\mathbf{E}\left\{\sum_{k\neq m} s_k \sum_n \sum_p w(p\Delta t + \tau_p) e^{j\frac{2\pi}{N}((k-m)n - mp)} e^{-j2\pi f_k \tau_n}\right\} \\ &= 0.\end{aligned}$$

APPENDIX E

GENERATION OF COLORED TIMING JITTER PROCESS USING LEVINSON-DURBIN'S ALGORITHM

In this work, we occasionally have to generate colored timing jitter sequence in the simulation. For instance, colored timing jitter processes with either the Gaussian correlation property ($\rho(t) = e^{-\beta t^2}$) or the exponential correlation property ($\rho(t) = e^{-a|t|^2}$) were extensively used in this thesis.

The basic approach in generating the colored timing jitter is to find filter coefficients yielding the correlation properties. Figure 25 below illustrates the general concept: We seek $h(n)$ that gives $\tau(n)$ the correlation property, $R(m)$, where $R(m)$

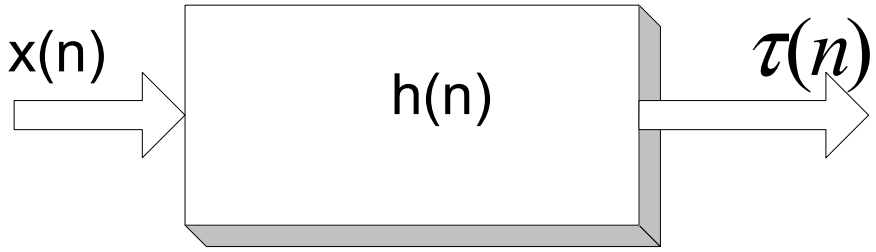

Figure 25. Generation of colored timing jitter

could be exponential, Gaussian, or any valid correlation function. The input to the filter, $x(n)$, is a zero-mean, unit variance white process. Now,

$$\begin{aligned} R(m) &= \mathbf{E}\{\tau(n)\tau(n+m)\} \\ &= \mathbf{E}\{\sum_l h(l)x(n-l) \cdot \sum_p h(p)x(n+m-p)\} \\ &= \sum_l \sum_p h(l)h(p)\mathbf{E}\{x(n-l)x(n+m-p)\} \end{aligned}$$

$$= \sum_{l}\sum_{p} h(l)h(p)\delta(m-p+l)$$

which simplifies to

$$R(m) = \sum_{l} h(l)h(m+l)$$

that is readily solved using the Levinson-Durbin's algorithm.

For the correlation properties considered in this work, the filter is normally an AR of order 2 with frequency response of

$$H(z) = \mathcal{Z}\{h(n)\} = \frac{1}{1-a_1 z^{-1}} \Longleftrightarrow h(n) = (a_1)^n.$$

In practice, the filter length is truncated such that the filter $h(n)$ is approximated by an FIR filter $\tilde{h}(n)$ and the colored jitter process is generated by convolution

$$\tau(n) = x(n) * \tilde{h}(n).$$

REFERENCES

[1] IEEE P802.15 meeting document.

[2] "Revision of part 15 of the commission's rules regarding ultra-wideband transmission systems," tech. rep., ET-Docket 98-153. FCC Notice of Proposed Rule Making.

[3] Balakrishnan, A., "On the problem of time jitter in sampling," *IEEE Trans. Info. Theory*, vol. 8, pp. 226–236, April 1962.

[4] Batra, A., "Multiband-ofdm physical layer proposal," *IEEE P802.15-03/268r2*, Nov. 2003.

[5] Batra, A., Balakrishnan, J., Aiello, G. R., and Foerster, J. R., "Design of a multiband ofdm system for realistic uwb channel environments," *IEEE Trans. Microwave Theory and Tech.*, vol. 52, pp. 2123–2138, Sept. 2004.

[6] Batra, A., Balakrishnan, J., Aiello, G. R., Foerster, J. R., and Dabak, A., "Design of a multiband ofdm system for realistic uwb channel environments," *IEEE Trans. Microwave Theory and Techniques*, vol. 52, pp. 2123–2138, Sept. 2004.

[7] Budge, M., Jr, and Gilbert, S., "Timing jitter spectrum in pulsed and pulsed doppler radars," *Proc. IEEE Souhteastcon*, pp. 1–4, April 1993.

[8] Chen, X. and Kiaei, S., "Monocycle shapes for ultra wideband system," *IEEE Int. Symposium Circuits and Sys.*, vol. 1, pp. 597–600, May 2002.

[9] Chong, C.-C., Kim, Y., and Lee, S.-S., "A modified s-v clustering channel model for the uwb indoor residential environment," *IEEE 61st Conf. on Veh. Tech., VTC 2005-Spring*, vol. 1, pp. 58–62, June 2005.

[10] Cox, D. C., "Delay doppler characteristics of multipath propagation at 910 mhz in suburban mobile radio environment," *IEEE Trans. on Antennas and Prop.*, vol. 20, pp. 625–635, Sept. 1972.

[11] Forgac, J. and Farkas, P., "Analysis of different uwb systems with timing jitter and isi in awgn channel," *SympoTIC'03 Joint First Workshop on Mobile Future and Symposium on Trends in Commun.*, pp. 51–54, Oct. 2003.

[12] Gao, X., Yao, R., and Feng, Z., "Multi-band uwb system with hadamard coding," *IEEE Veh. Tech. Conf.*, vol. 2, pp. 1288–1292, Oct. 2003.

[13] Gezici, S., Molisch, A. F., Poor, H. V., and Kobayashi, H., "The trade-off between processing gains of impulse radio systems in the presence of timing jitter," *IEEE 2004 International Conf. on Commun.*, vol. 6, pp. 3596–3600, June 2004.

[14] Gradshteyn, L. and Ryzhik, I., *Table of Integrals, Series, and Products*. San Diego, CA: Academic Press, 6th ed., 2000.

[15] Guvenc, I. and Arslan, H., "Performance evaluation of uwb systems in the presence of timing jitter," *IEEE Conf. on UWB Systems and Tech.*, pp. 136–141, Nov. 2003.

[16] Harjani, R., Harvey, J., and Sainati, R., "Analog/rf physical layer issues for uwb systems," *Proc. 17th Int. Conf. VLSI Design*, pp. 941–948, Jan. 2004.

[17] Hor, P. B., Ko, C. C., and Zhi, W., "Ber performance of pulsed uwb system in the presence of colored timing jitter," *International Workshop on UWBST & IWUWBS*, pp. 293–297, May 2004.

[18] Huang, H., Yin, H., Wei, G., and Zhu, J., "A jitter-robust high data rate impulse radio system with an orthogonal sinusoidal correlation receiver," *IEEE Intern. Conf. on Wireless Network, Commun. and Mobile Comp.*, vol. 2, pp. 1220–1224, June 2005.

[19] Kamoun, M., Buzenac, V., de Courville, M., and Duhamel, P., "A digital jitter cancelling algorithm for ppm impulse radio ultra-wide-band systems," *IEEE Intern. Conf. on Commun.*, vol. 1, pp. 412–416, May 2005.

[20] Li, Y. G., Jr., L. J. C., and Sollenberger, N. R., "Robust channel estimation for ofdm systems with rapid dispersive fading channels," *IEEE Trans. Commun.*, vol. 46, pp. 902–915, July 1998.

[21] Li, Y. G., Molisch, A., and Zhang, J., "Practical approaches to channel estimation and interference suppression for ofdm based uwb communications," *to appear in IEEE Trans. Wireless Commun.*

[22] Li, Y. G., Molisch, A. F., and Zhang, J., "Channel estimation and signal detection for uwb," *Int. Symposium Wireless Personal Multimedia Commun.*, October 2003.

[23] Li, Y. G., Molisch, A. F., and Zhang, J., "Practical approaches to channel estimation and interference suppression for ofdm based uwb communications," *Proc. IEEE Circuits and Sys. Symposium Emerging Tech.: Frontiers of Mobile and Wireless Commun.*, vol. 1, pp. 21–24, May-June 2004.

[24] Li, Y. G. and Sollenberger, N., "Adaptive antenna arrays for ofdm systems with cochannel interference," *IEEE Trans. Commun.*, vol. 47, pp. 217–229, Feb. 1999.

[25] Liu, B. and Stanley, T., "Error bounds for jittered sampling," *IEEE Trans. Auto. Control*, vol. 10, pp. 449–454, Oct. 1965.

[26] Liu, T. and Wang, C., "A 1-4 ghz dll based low-jitter multi-phase clock generator for low-band ultra-wideband application," *IEEE Asia-Pacific Conf. on Adv. Sys. Integrated Circuits*, pp. 330–333, Aug. 2004.

[27] Lottici, V., D'Andrea, A., and Mengali, U., "Channel estimation for ultra-wideband communications," *IEEE J. Select. Areas Commun.*, vol. 20, pp. 1638–1645, Dec. 2002.

[28] Lovelace, W. M. and Townsend, J. K., "The effects of timing jitter and tracking on the performance of impulse radio," *IEEE J. Selected Areas Commun.*, vol. 20, pp. 1646–1651, Dec. 2002.

[29] Manoj, K. N. and Thiagarajan, G., "The effect of sampling jitter in ofdm systems," *IEEE International Conf. on Commun.*, pp. 2061–2065, May 2003.

[30] Michael, L., Ghavami, M., and Kohno, R., "Multiple pulse generator for ultra-wideband communication using hermite polynomial based orthogonal pulses," *IEEE Conf. UWB Sys. and Tech.*, pp. 47–51, May 2002.

[31] Molisch, A. F., Li, Y. G., and Nakache, Y., "A low-cost time-hopping impulse radio system for high data rate transmission," *submitted for publishing in IEEE Journal.*

[32] Onunkwo, U. and Li, Y. G., "On the optimum pulse-position modulation index for ultra-wideband communication," *Proc. IEEE Circuits and Sys. Symposium Emerging Tech.: Frontiers of Mobile and Wireless Commun.*, vol. 1, pp. 77–80, May-June 2004.

[33] Popescu, D., Yaddanapudi, P., and Kondadasu, R., "Ofdm versus time-hopping in multiuser ultra wideband communication systems," *IEEE 61st Veh. Tech. Conf.*, vol. 2, pp. 1406–1410, June 2005.

[34] Saad, S. S., "Analysis of accumulated timing-jitter in the time domain," *IEEE Trans. on Instr. and Meas.*, vol. 47, pp. 69–73, Feb. 1998.

[35] Saberinia, E. and Tewfik, A. H., "Multi-user uwb-ofdm communications," *IEEE Pacific Rim Conf. Commun., Comp. and Signal Processing*, vol. 1, pp. 127–130, Aug. 2003.

[36] Sakamoto, T. and Sato, T., "An estimation method of target location and scattered waveforms for uwb pulse radar systems," *Proc. IEEE Int. Geoscience and Remote Sensing Symposium*, vol. 6, pp. 4013–4015, July 2003.

[37] Tang, J. and Parhi, K. K., "On the power spectrum density and parameter choice of multi-carrier uwb communications," *37th Asilomar Conf. Signals, Sys. & Comp.*, vol. 2, pp. 1230–1234, Nov. 2003.

[38] Tomba, L. and Krzymien, W. A., "A model for the analysis of timing jitter in ofdm systems," *IEEE International Conf. on Commun.*, vol. 3, pp. 1227–1231, June 1998.

[39] Walden, R. H., "Analog-to-digital converter survey and analysis," *IEEE J. Select. Areas Commun.*, vol. 17, pp. 539–550, April 1999.

[40] Wang, D., Liu, D., and Yue, G., "A novel modification method for ieee802.15.3a channel model," *Conf. on Ultrawideband Systems and Tech.*, pp. 86–90, May 2004.

[41] Weinstein, S. B. and Ebert, P. M., "Data transmission by frequency-division multiplexing using the discrete fourier transform," *IEEE Trans. Commun. Tech.*, vol. 19, pp. 628–634, Oct. 1971.

[42] Win, M., "On the power spectral density of digital pulse streams generated by m-ary cyclostationary sequences in the presence of stationary timing jitter," *IEEE Trans. Commun.*, vol. 46, pp. 1135–1145, Sept. 1998.

[43] Winters, J. H., "Signal acquisition and tracking with adaptive arrays in the digital mobile radio system is-136 with flat fading," *IEEE Trans. Veh. Technol.*, vol. 42, pp. 377–384, Nov. 1993.

[44] Zogakis, T. N. and Cioffi, J. M., "The effect of timing jitter on the performance of a discrete multitone system," *IEEE Trans. Commun.*, vol. 44, pp. 799–808, July 1996.

VITA

Uzoma Onunkwo was born in Knoxville, Tennessee (USA). He received his B. Eng. degree in 2001 from the Department of Electrical and Computer Engineering with First-In-Class honor at Stevens Institute of Technology, New Jersey and his Masters degree in 2002 from the Department of Electrical and Computer Engineering at Georgia Institute of Technology, Georgia. In 2001, he worked as an intern with Lucent Bell Laboratories in the Speech Processing and Multimedia Group, and in 2005 as an intern with M.I.T. Lincoln Laboratories in the Advanced Satellite Communication group. His research interests include channel modeling & estimation, signal modulation & detection, and error-correction coding with emphasis on ultra wideband systems and orthogonal frequency division multiplexing.